

Molecular templating using titanium(IV) (oxo)alkoxides and titanium(IV) (oxo)aryloxides†‡

Abdelhamid Senouci, Mfeddel Yaakoub, Clarisse Huguenard and Marc Henry*

Université Louis Pasteur, Laboratoire de Chimie Moléculaire et de RMN du Solide, Institut Le Bel, 4, Rue Blaise Pascal, 67070 Strasbourg Cedex, France

Received 4th May 2004, Accepted 19th July 2004

First published as an Advance Article on the web 24th September 2004

Crystalline materials obtained by reacting titanium(IV) isopropoxide (**1**) with widely different ligands such as 1,3-propanediol, 2,2'-biphenol or triphenylacetic acid using acetone as a solvent have been characterised using single-crystal X-ray diffraction, ^1H , ^{13}C and ^{17}O NMR spectroscopies and theoretical modelling. In the case of the previously described $[\text{Ti}_3(\mu_3\text{-O})(\text{OPr}^i)_4(\mu\text{-OPr}^i)_3\{\text{Me}_2\text{C}(\text{O})\text{CH}=\text{C}(\text{O})\text{CH}_2\text{C}(\text{O})\text{Me}_2\}]$ complex (**2**), the importance of the simultaneous use of HSQC, HBM C and ROESY techniques for a full spatial attribution of all resonances was demonstrated. The optimised molecular structure of (**2**) and its associated dynamics have also been used to demonstrate that more shielded ^1H and ^{13}C resonances and shorter relaxation times were expected for more rigid bridging OR groups relative to terminal ones. A templating effect linked to the steric decompression that may occur when the rather constrained molecular structure of $[\text{Ti}_3(\mu_3\text{-O})(\mu_3\text{-OPr}^i)(\mu\text{-OPr}^i)_3(\text{OPr}^i)_6]$ (**3**) meets acetone molecules in their enol form, $(\text{3}) + 3 \text{CH}_2=\text{C}(\text{OH})\text{CH}_3 \rightarrow (\text{2}) + 3 \text{HOPr}^i$, is proposed, explaining why exactly three acetone molecules should undergo aldol condensation and why new complexes such as $[\text{Ti}_3(\mu_3\text{-O})(\mu_3\text{-OH})(\text{OPr}^i)_6(\mu\text{-OPr}^i)_3]$ (**4**) or $[\text{Ti}_3(\mu_3\text{-O})(\mu\text{-OOCPh}_3)_2(\mu\text{-OPr}^i)_3(\text{OPr}^i)_5]$ (**5**) may be isolated and characterised.

Introduction

Titanium(IV) oxide is a very attractive material owing to its cheapness, its low toxicity towards living cells and its interesting semi-conducting properties.¹ Following a bottom-up approach it may be easily synthesized using sol-gel processing after hydrolysis and condensation of titanium(IV) alkoxides.^{1,2} By contrast very few reports of sol-gel processes involve the use of titanium(IV) aryloxides, even though such molecular complexes are widely used as catalysts in organic chemistry or as building blocks in supramolecular chemistry.^{1,3,4} In fact, from its very beginning, sol-gel processing of oxide materials involved the formation of self assembled structures displaying various sizes and shapes (oxo-alkoxides and oxo-aryloxides). It is then striking to see that sol-gel chemistry is currently in the uncomfortable position of relying heavily on self-assembly processes without knowing the basic rules that govern the formation of the various building blocks that may be used, for instance, in the design of hybrid organic-inorganic materials. In the past years our group has spent considerable efforts in trying to unveil these self-assembly rules by reacting titanium(IV) alkoxides $\text{Ti}(\text{OR})_4$ ($\text{R} = \text{Et}, \text{Pr}^i, \text{Bu}^n$) with carefully selected ligands bearing two, three or four OH-groups linked to three different kinds of organic moieties: methylene CH_2 , benzene ring and carbonyl $\text{C}=\text{O}$ groups. Fig. 1 gathers what have been observed after characterisation of reaction products through single-crystal X-ray diffraction.³⁻⁷ It emerges from Fig. 1 that when the incoming ligand shares some structural feature with the basic tetrameric core typical of titanium(IV) alkoxides^{8,9} this core is not broken allowing to speak of molecular recognition (face-recognition in the case of tris(hydroxymethyl)nitromethane or edge-recognition in the case of 2,6-bis(hydroxymethyl)-*p*-cresol). Further analysis of these structures in terms of steric

hindrance, electronic densities and packing energies using the non-empirical PACHA (Partial Atomic CHarges) software,¹⁰ has allowed the establishment of two general self-assembly rules:

i) First, bridging OR-groups are systematically more basic than terminal ones and thus should be selectively attacked or substituted by protic XOH reagents. This rule helps to explain the absence of clear structural relationships among the various hydrolysis products of titanium(IV) alkoxides and allows structural relationships among observed structures to be established.

ii) Second, a reduction in coordination is systematically associated with more electrophilic Ti-atoms and with stronger chemical bonds. This fact associated with the high lability of the Ti-O bond helps to explain the frequent reduction in coordination numbers that may occur on going from the solid state (crystalline structures) to the solution. This points out the importance of ^1H , ^{13}C and ^{17}O NMR spectroscopy both in solution and in the solid state for a full characterisation of both structural and dynamical behaviour of these systems.

However, most detailed NMR studies devoted to these compounds¹¹⁻¹⁴ remain at a qualitative level. For instance, it is commonly observed that fully resolved ^{13}C NMR spectra might be recorded calling for the establishment of a one to one correspondence between X-ray labels and NMR peaks. But until now, we have not been able to find in the literature a single example of such a correspondence, a surprising observation in view of the large availability of powerful NMR pulse sequences. Consequently, we show in this study how such a correspondence may be established for the first time through the simultaneous use of X-ray diffraction, NMR and modelling techniques. Moreover, as we are deeply interested in molecular recognition we have selected the interesting case of the reaction occurring when titanium(IV) isopropoxide $\text{Ti}(\text{OPr}^i)_4$ (**1**) is dissolved into acetone. According to previous studies^{15,16} a complex (**2**) formulated as $[\text{Ti}_3(\mu_3\text{-O})(\text{OPr}^i)_4(\mu\text{-OPr}^i)_3\{\text{Me}_2\text{C}(\text{O})\text{CH}=\text{C}(\text{O})\text{CH}_2\text{C}(\text{O})\text{Me}_2\}]$ may be isolated, but it was characterised by a large crystallographic disorder

† Basis of a presentation given at Materials Discussion No. 7, 13-15th September 2004, London, UK.

‡ Electronic supplementary information (ESI) available: theoretical structure for compound (**2**) computed and used for modeling NMR data (see text). See <http://www.rsc.org/suppdata/jm/b4/b406696k/>

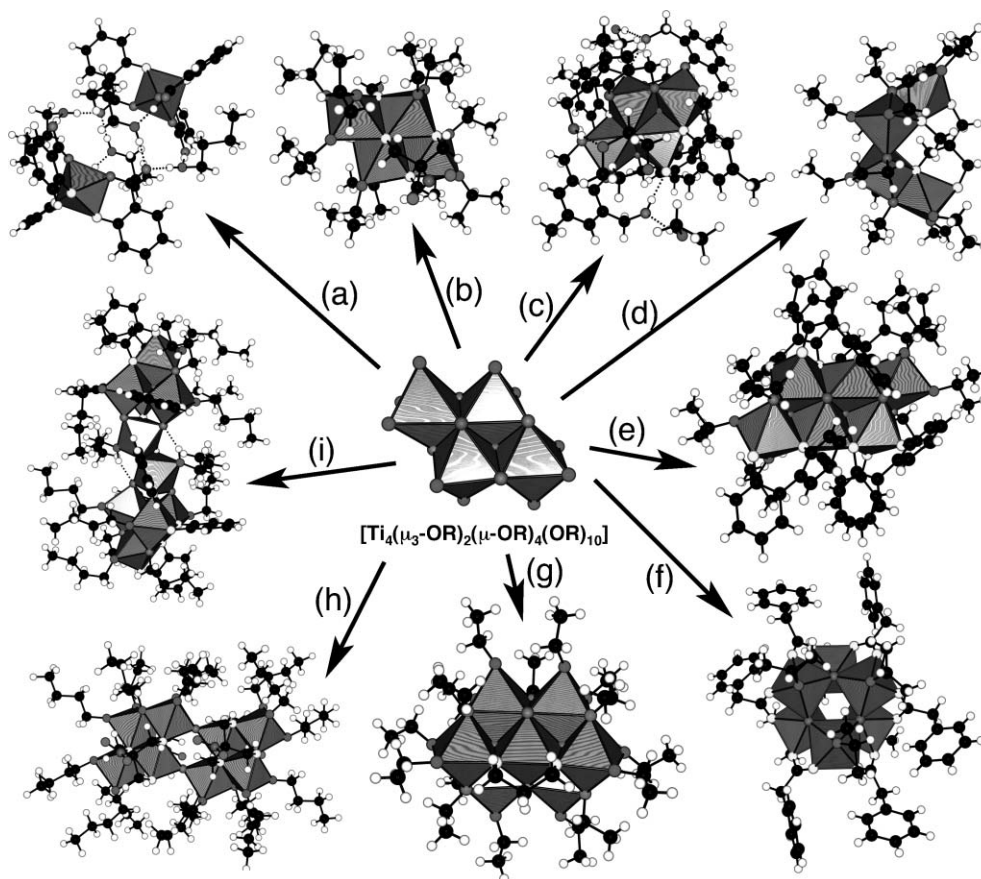


Fig. 1 Molecular recognition or reorganisation of the basic tetrameric structure of titanium(IV) alkoxides (centre). (a) Breaking down to monomers and formation of $\{(\Lambda, \Delta)\text{-}[\text{Ti}(\text{sal})(\text{salH})_2](^n\text{BuOH})_2\}_2$ after reaction with salicylic acid (H_2sal). (b) Conservation with selective substitution of $\mu_3\text{-OR}$ bridges and formation of $[\text{Ti}_4(\text{OR})_{10}(\mu_3\text{-thmmm})_2]$ ($\text{R} = \text{Et}, \text{Pr}^i$) after reaction with tris(hydroxymethyl)nitromethane (H_3thmmm). (c) Conservation with substitution of all alkoxy groups and formation of $\{[\text{Ti}_2(\mu_3\text{-O})(\mu\text{-bhmpe})(\mu\text{-Hbhmpe})(\eta^2\text{-H}_2\text{bhmpe})]\cdot\text{EtOH}\cdot\text{C}_4\text{H}_8\text{O}_2\}_2$ after reaction with 2,6-bis(hydroxymethyl)-*p*-cresol (H_2bhmpe). (d) Linearization with selective substitution of $\mu_3\text{-OR}$ bridges and formation of $[\text{Ti}_4\{\mu_4\text{-}(\text{OCH}_2)\text{C}\}(\mu\text{-OEt})_4(\text{OEt})_8]$ after reaction with pentaerythritol. (e) Augmentation with selective substitution of OR bridges and formation of $[\text{Ti}_6(\mu_3\text{-O})_4(\mu\text{-bipol})_6(\text{OPr}^i)_4(^i\text{PrOH})_2]$ after reaction with 2,2'-biphenol (H_2bipol). (f) Reorganisation to trimers and formation of $[\text{Ti}_6(\mu_3\text{-O})_6(\mu\text{-OOCCH}_2\text{Ph})_6(\text{OPr}^i)_6]$ after reaction with phenylacetic acid. (g) Selective substitution of $\mu\text{-OR}$ bridges in the first hydrolysis product of titanium(IV) tetraethoxide and formation of $[\text{Ti}_7(\mu_4\text{-O})_2(\mu_3\text{-O})\{\mu\text{-O}(\text{CH}_2)_3\text{O}\}(\mu\text{-OEt})_6(\text{OEt})_{12}]$ after reaction with 1,3-propanediol. (h) Conservation with selective substitution of $\mu_3\text{-OR}$ bridges and selective oxalation leading to $\{[\text{Ti}_4(\mu\text{-O})(\mu_3\text{-thmmm})_2(\mu\text{-OBu}^n)(\text{OBu}^n)_7]_2\}$ after reaction with H_3thmmm . (i) Breaking down to dimers and reorganisation leading to $[\text{Ti}_{10}(\mu_4\text{-O})_2(\mu\text{-O})_4(\mu_3\text{-cat})_2(\mu\text{-cat})_6(\text{OBu}^n)_{12}(^n\text{BuOH})_2]$ after reaction with 1,2-dihydroxybenzene (H_2cat).

and led to eight well-resolved methine resonances in the ^{13}C NMR spectrum that do not fit with the X-ray structure evidencing only seven isopropoxy groups. But, let's notice that for X-ray diffraction there should exist no differences between (2) displaying a $\text{Ti}_3\text{O}_{11}\text{C}_{30}\text{H}_{64}$ stoichiometry and the first hydrolysis product of (1) $[\text{Ti}_3(\mu_3\text{-O})(\mu_3\text{-OPr}^i)(\mu\text{-OPr}^i)_3(\text{OPr}^i)_6]$ (3) displaying a $\text{Ti}_3\text{O}_{11}\text{C}_{30}\text{H}_{70}$ stoichiometry. One may then wonder if the formation of (2) could be due to a true molecular templating effect involving (3) and acetone molecules rather than a mere isolation of a coordinated intermediate fragment of aldol coupling. This has led us to reconsider what could happen when (1) is reacted with some hydroxylated ligands in the presence of acetone. As a corollary, as (2), (3) as well as $[\text{Ti}_3(\mu_3\text{-O})(\mu_3\text{-OH})(\text{OPr}^i)_6(\mu\text{-OPr}^i)_3]$ (4) share exactly the same $[\text{Ti}_3(\mu_3\text{-O})(\mu\text{-OPr}^i)_3]$ core, it was mandatory to get also an unambiguous full assignment of the ^{13}C NMR spectrum of (2).

Materials and methods

The starting material was titanium(IV) isopropoxide $\text{Ti}(\text{OPr}^i)_4$ (1) (F.W. = $284.28 \text{ g mol}^{-1}$, $d = 0.955 \text{ g cm}^{-3}$) bought from Aldrich (20,527-3; CAS 546-68-9) and used without any further purification.

Synthesis of (2) $[\text{Ti}_3(\mu_3\text{-O})(\text{OPr}^i)_4(\mu\text{-OPr}^i)_3\{\text{Me}_2\text{C}(\text{O})\text{CH}=\text{C}(\text{O})\text{CH}_2\text{C}(\text{O})\text{Me}_2\}]$

This complex may be easily synthesised by mixing (1) with acetone using a $\text{Me}_2\text{CO}/\text{Ti}$ molar ratio between 4 and 20. Colourless crystals of (2) used for ^{17}O NMR measurements were prepared by stirring (1) (2 mL, 6.7 mmol) and propan-2-one (10 mL, 136 mmol) in a closed vessel after standing overnight. This preparation method is however not suitable to get pure single-crystals of (2). A much better way is to stir (15 minutes) in a closed vessel (1) (1 mL, 3.4 mmol) with propan-2-one (10 mL, 136 mmol) containing 0.4 g (1.69 mmol) of triphenylacetic acid. Colourless crystals are also obtained after standing these solutions overnight.

Synthesis of (4) $[\text{Ti}_3(\mu_3\text{-O})_2(\mu\text{-OPr}^i)_3(\text{OPr}^i)_6]$

This complex was synthesised after stirring (15 minutes) in a closed vessel (1) (0.5 mL, 1.7 mmol) with a solution (10 mL) of propan-2-ol containing 50 vol% propan-2-one and 0.2 g (0.9 mmol) of triphenylacetic acid. Yellow prismatic crystals suitable for X-ray diffraction were obtained after standing these solutions overnight.

Crystal data. $\text{C}_{27}\text{H}_{63}\text{O}_{11}\text{Ti}_3$, $M = 707.50$, hexagonal, space group $R3_2$ (no. 155), $a = 17.9240(6) \text{ \AA}$, $c = 20.966(1) \text{ \AA}$,

$U = 5833.5(4) \text{ \AA}^3$, $T = 173\text{K}$, $Z = 6$, $\mu(\text{Mo-K}\alpha) = 0.647 \text{ cm}^{-1}$, 3888 reflections measured (1838 unique), 1184 observed reflections [$I \geq 3\sigma(I)$], $R[I \geq 3\sigma(I)] = 0.100$, $R_w(F, \text{all reflections}) = 0.168$, $\text{GOF} = 1.496$. Refinement using the $R-3m$ space-group was attempted but was not successful. \S

In another synthesis (**1**) (1 mL, 3.8 mmol) was stirred with a solution (10 mL) of propan-2-one containing 25 mg (0.33 mmol) of propane-1,3-diol. Yellow prismatic crystals suitable for X-ray diffraction were obtained after standing these solutions overnight.

Crystal data. $\text{C}_{27}\text{H}_{63}\text{O}_{11}\text{Ti}_3$, $M = 707.50$, monoclinic, space group $C2/m$ (no. 12), $a = 17.3967(4) \text{ \AA}$, $b = 17.9221(4) \text{ \AA}$, $c = 12.4873(1) \text{ \AA}$, $\beta = 92.465(9)^\circ$, $U = 3889.8(2) \text{ \AA}^3$, $T = 173\text{K}$, $Z = 4$, $\mu(\text{Mo-K}\alpha) = 0.639 \text{ cm}^{-1}$, 14509 reflections measured (4112 unique), 3605 observed reflections [$I \geq 3\sigma(I)$], $R[I \geq 3\sigma(I)] = 0.094$, $R_w(F, \text{all reflections}) = 0.149$, $\text{GOF} = 1.797$.

Synthesis of (**5**) $[\text{Ti}_3(\mu_3\text{-O})(\mu\text{-OOCPh}_3)_2(\mu\text{-OPr}^i)_3(\text{OPr}^i)_5]$

This complex was synthesised after stirring (15 minutes) in a closed vessel (**1**) (1 mL, 3.4 mmol) with a solution (10 mL) of propan-2-ol containing 50 vol% propan-2-one and 0.4 g (1.69 mmol) of triphenylacetic acid. Colourless crystals suitable for X-ray diffraction were obtained after standing these solutions overnight.

Crystal data. $\text{C}_{65}\text{H}_{64}\text{O}_{13}\text{Ti}_3$, $M = 1185.86$, triclinic, space group $P-1$ (no. 2), $a = 11.8950(2) \text{ \AA}$, $b = 12.9300(3) \text{ \AA}$, $c = 22.4330(4) \text{ \AA}$, $\alpha = 89.2040(16)^\circ$, $\beta = 86.2390(15)^\circ$, $\gamma = 72.2170(16)^\circ$, $U = 3278.25(11) \text{ \AA}^3$, $T = 293\text{K}$, $Z = 2$, $\mu(\text{Mo-K}\alpha) = 0.414 \text{ cm}^{-1}$, 49393 reflections measured (18281 unique), 13777 observed reflections [$I \geq 2\sigma(I)$], $R[I \geq 2\sigma(I)] = 0.080$, $R_w(F^2, \text{all reflections}) = 0.2541$, $\text{GOF} = 1.135$.

^1H NMR (CDCl_3 , 500 MHz, 300 K). δ 0.67 (3H, d, $J = 6.4 \text{ Hz}$, OCHMe_2), 0.77 (3H, d, $J = 6.4 \text{ Hz}$, OCHMe_2), 0.78 (3H, d, $J = 6.4 \text{ Hz}$, OCHMe_2), 0.81 (3H, d, $J = 6.4 \text{ Hz}$, OCHMe_2), 0.85 (3H, d, $J = 6.4 \text{ Hz}$, OCHMe_2), 0.90 (3H, d, $J = 6.4 \text{ Hz}$, OCHMe_2), 1.02 (3H, d, $J = 6.4 \text{ Hz}$, OCHMe_2), 1.12 (3H, d, $J = 6.4 \text{ Hz}$, OCHMe_2), 4.2 (1H, sept, $J = 6.4 \text{ Hz}$, OCHMe_2), 4.48 (2H, sept, $J = 6.4 \text{ Hz}$, OCHMe_2), 4.55 (2H, sept, $J = 6.4 \text{ Hz}$, OCHMe_2), 4.60 (1H, sept, $J = 6.4 \text{ Hz}$, OCHMe_2), 4.66 (2H, sept, $J = 6.4 \text{ Hz}$, OCHMe_2), 7.00–7.40 (5 H_{arom} , $(\text{C}_5\text{H}_5\text{C})_3\text{CCOO}$).

^{13}C NMR (CDCl_3 , 500 MHz, 300 K). δ 23.7 (OCHMe_2), 24.5 (OCHMe_2), 24.7 (OCHMe_2), 24.9 (OCHMe_2), 25.3 (OCHMe_2), 25.5 (OCHMe_2), 25.7 (OCHMe_2), 26.4 (OCHMe_2), 68.7 ($\text{Ph}_3\text{CCOO-Ti}$), 76.2 (OCHMe_2), 76.2 (OCHMe_2), 76.6 (OCHMe_2), 76.9 (OCHMe_2), 77.9 (OCHMe_2), 77.9 (OCHMe_2), 79.3 (OCHMe_2), 79.3 (OCHMe_2), 125.8 ($(p\text{-C}_5\text{H}_5\text{C})_3\text{CCOO-Ti}$), 127.0 ($(m\text{-C}_5\text{H}_5\text{C})_3\text{CCOO-Ti}$), 131.1 ($(o\text{-C}_5\text{H}_5\text{C})_3\text{CCOO-Ti}$), 144.5 ($(\text{C}_5\text{H}_5\text{C})_3\text{CCOO-Ti}$), 179.2 ($(\text{Ph})_3\text{CCOO-Ti}$).

NMR measurements

^1H and ^{13}C T_1 measurements, as well as ^{17}O spectra were obtained at ambient temperature. For all other measurements the sample temperature was regulated at 273 K. ^{13}C T_1 determination and ^{17}O acquisition were made on a Bruker Avance-400 spectrometer, operating at 100.61 MHz and 54.24 MHz, with a $^1\text{H}/^{13}\text{C}$ 10 mm probe and a $^1\text{H}/\text{X}$ 10 mm probe, for ^{13}C and ^{17}O respectively. All other 1D and 2D

solution spectra were recorded on a Bruker Avance-500 spectrometer, operating at 500.13 MHz for ^1H and 125.7 MHz for ^{13}C , using a $^1\text{H}/^{13}\text{C}$ 5 mm gradient-probe. We used a gradient selected version (gs-) for each type of 1D and 2D pulse sequence except for ROESY where the coherence pathway selection is obtained by a classical phase cycling method.

The solvent signal was taken as a secondary reference for ^1H and ^{13}C chemical shifts (7.26 ppm for C^1HCl_3 residue and 77 ppm for $^{13}\text{CDCl}_3$, relative to TMS). A water sample served as an external reference for ^{17}O chemical shift.

8 Scans and 1560 scans were accumulated for 1D ^1H and ^{13}C spectra at 273 K respectively. The ^{17}O spectrum was obtained with 252997 scans and a 0.1 s repetition time. T_1 measurements involved a classical inversion-recovery sequence, with ^1H decoupling in the case of ^{13}C . We adopted a 15 s repetition time with 8 scans for ^1H and 30 s with 88 scans for ^{13}C .

A homonuclear ^1H - ^1H scalar correlation spectrum was obtained using a gs-DQF-COSY pulse sequence (for Double Quantum Filtered Correlation Spectroscopy)^{17,18} with 4 scans, 2.5 s as repetition time, and 512 increments for indirect dimension. A second homonuclear ^1H - ^1H correlation spectrum intended to explore the dipolar H,H correlations was recorded with a ROESY pulse sequence (Rotating frame Overhauser Enhancement Spectroscopy) using off-resonance adiabatic pulses for spin-lock.¹⁹ Acquisition parameters were 4 scans, 2 s as repetition time, 256 increments for indirect dimension and a total mixing spin-lock duration of 300 ms suitable for the correlation time one can expect, considering the size of the molecular entity under study.

A heteronuclear ^1H - ^{13}C *via* $^1J_{\text{C-H}}$ scalar correlation spectrum was acquired with a gs-HSQC pulse sequence (Heteronuclear Single Quantum Coherence),²⁰ 4 scans, 2 s as repetition time, 1024 increments in ^{13}C dimension, a delay $1/4J = 1.56 \text{ ms}$ corresponding to mean $^1J_{\text{C-H}} = 160 \text{ Hz}$.

A heteronuclear ^1H - ^{13}C long range scalar correlation spectrum, showing essentially $^2J_{\text{C-H}}$ and $^3J_{\text{C-H}}$ H,C correlations in our case, was obtained with a gs-HMBC pulse sequence (Heteronuclear Multiple Bond Correlation).²¹ As $^1J_{\text{C-H}}$ correlations cannot be totally suppressed by the low-pass J -filter, the 2D spectrum exhibit some residual one-bond H,C correlation peaks appearing as doublets. Acquisition parameters were 16 scans, 2 s as repetition time, 1024 increments in ^{13}C dimension and a delay $1/2J = 3.12 \text{ ms}$ corresponding to mean $^1J_{\text{C-H}} = 160 \text{ Hz}$.

Molecular and crystal structure optimisation

In order to get a structural model free of disorder we have used the non-empirical PACHA formalism¹⁰ that is able to derive realistic interaction energies,^{22–31} or NMR parameters^{32,33} after optimisation under constrained bond lengths of atomic coordinates. The homemade graphical interface used for all the computations is freely available.³⁴ The starting geometry was the Ti_3O_{11} core plus the rigid backbone of the enolate ligand (C-C-C=C-C) and the seven methine C-atoms extracted from the X-ray crystal structure. In order to get atomic charges that depend only on the relative positions of the organic groups in the structure and not on unavoidable errors related to the refinement of the X-ray data, all C-atoms directly bonded to oxygen are moved along the experimental C–O direction in order to get the same standard C–O bond length (143 pm). All the remaining mobile parts (18 C-atoms and 64 H-atoms) were then grafted on this rigid core, relying on standard Z-matrix techniques,³⁵ using constant C–C (153 pm) and C–H bond lengths with ideal tetrahedral geometry around aliphatic C-atoms and trigonal planar geometry for olefinic C-atoms. Four kinds of standard C–H bond lengths were used: 106 pm (methyl), 108 pm (methine sp^2), 109 pm (methylene) and 110 pm (methine sp^3). Optimum values for the 164 variable angles were then obtained after minimisation³⁶ of the total energy

\S CCDC reference numbers 240743, 244826 and 244827. See <http://www.rsc.org/suppdata/jm/b4/b406696k/> for crystallographic data in .cif or other electronic format.

computed as the sum of three terms: the steric energy relying on *ab initio* atom–atom potentials derived from the Gordon–Kim electron gas model,³⁷ the London dispersive energy derived again from the Gordon–Kim electron gas model³⁷ and the electrostatic balance¹⁰ computed from the partial charge distribution associated with each move in angles. As no *ab initio* data were available for Ti-atoms, we have used exponential forms fitted to tight-binding potentials.³⁸ Dispersive contributions arising from interactions with Ti-atoms were assumed to be negligible as all these atoms are deeply buried in rigid TiO₆ octahedra whose geometry is fixed by X-ray diffraction. It is worth noting that the whole charge distribution is recomputed after each alteration of atomic coordinates, leading to a rigorous non-empirical way of taking into account polarisation effects that are known to be so important for molecular crystals. In order to probe the effect of intermolecular interactions on NMR parameters, the crystal structure of (2) has also been optimised using the experimental *R*–3*m* space group symmetry. Owing to the high symmetry, only positions of four C-atoms and 18 H-atoms (corresponding to a total of 44 angles) have to be optimised in order to define the positions of the 18 methyl groups and the atomic coordinates of the 64 H-atoms.

Computation of electric field gradients (efg)

Owing to their non-spherical symmetry quadrupolar nuclei such as ¹⁷O are able to interact with any electric field gradient, leading to quadrupolar patterns in the solid state and line broadening in solution. This interaction is usually characterized by the quadrupolar coupling constant $\chi = eQq_{zz}/h$, with e the elementary charge, h the Planck constant, Q the quadrupolar moment of the nucleus ($Q = -0.0256 \times 10^{-28} \text{ m}^2$ for the ¹⁷O nucleus) and q_{zz} the largest principal value of the efg tensor. The internal contribution EFG_{int} arising from the non-spherical filling of valence s-, p- or d-atomic orbitals centred on the quadrupolar nucleus has been empirically evaluated after a Townes–Dailey analysis,³⁹ based on the field gradient q_{210} at the ¹⁷O nucleus generated by a single electron in the 2p_z AO ($e^2Qq_{210}/h = 20.69 \text{ MHz}$ for ¹⁷O nucleus).^{40,41} The total wave function $|\Psi_n\rangle$ for a central O-atom having 2s and 2p-orbitals overlapping with 4 ligands' MO $|\phi_n\rangle$ was written as:

$$|\Psi_n\rangle = \alpha \left(a_{ns}|2s\rangle + a_{nx}|2p_x\rangle + a_{ny}|2p_y\rangle + a_{nz}|2p_z\rangle \right) + \sqrt{1-\alpha^2}|\phi_n\rangle \quad (1)$$

Knowledge of the orbital population p_n of each MO allows us then to write for the *xx* principal component of the efg tensor:

$$q_{xx} = q_{210} \sum_{n=1}^4 p_n \left[a_{nx}^2 - \frac{1}{2} (a_{ny}^2 + a_{nz}^2) \right] \quad (2)$$

Two other similar relations holds for the last components q_{yy} and q_{zz} after cyclic permutation of the (x,y,z) labels. In the case of symmetric μ_n -oxo bridges ($n = 2, 3, 4$), we have assumed tetrahedral bonds (*i.e.* $a_{ni} = \pm 1/2$) with an equal sharing of the electronic density ($p_1 = p_2 = p_3 = p_4 = p$) leading to $q_{xx} = q_{yy} = q_{zz} = 0$. For such situations, the only source of electric field gradient q_{zz}^{ext} comes from the embedding of the quadrupolar nuclei in a molecule or a lattice displaying alternating positive and negative atomic charges with a Sternheimer anti-shielding factor $|1 - \gamma_\infty|$ modelling the deformation of core orbitals: $\chi(^{17}\text{O}/\text{MHz}) = 0.0619 \times |(1 - \gamma_\infty)q_{zz}^{\text{ext}}(\text{V} \cdot \text{\AA}^2)|$.³² For terminal alkoxo groups (partial charge q_{O_t} on O-atoms) characterised by two non-bonding OM holding 2 electrons ($p_1 = 2, a_{1z} = 1, a_{1x} = a_{1y} = a_{1s} = 0$) and ($p_2 = 2, a_{2y} = 1, a_{2x} = a_{2z} = a_{2s} = 0$), a covalent bond was assumed between carbon and oxygen ($p_3 = 1$) and a polar bond between oxygen and titanium ($p_4 = 1 - q_{\text{O}_t}$) with ($a_{3s}^2 = a_{3x}^2 = a_{4s}^2 = a_{4x}^2 = 1/2, a_{3y}^2 = a_{3z}^2 = a_{4y}^2 = a_{4z}^2 = 0$).

Applying eqn. (2) then leads to a symmetric efg tensor $q_{yy} = q_{zz} = q_{210}(1 + q_{\text{O}_t}/2)/2$ with its maximum principal value along the x-direction $q_{xx} = -q_{210}(1 + q_{\text{O}_t}/2)$. For the bridging μ -OR case, characterised by one non-bonding OM holding 2 electrons ($p_1 = 2, a_{1z} = 1, a_{1x} = a_{1y} = a_{1s} = 0$) and trigonal geometry ($a_{2s}^2 = a_{3s}^2 = a_{4s}^2 = 1/3, a_{2x}^2 = 2/3, a_{3x}^2 = a_{4x}^2 = 1/6, a_{3y}^2 = a_{4y}^2 = 1/2, a_{2y}^2 = a_{2z}^2 = a_{3z}^2 = a_{4z}^2 = 0$), a covalent bond was assumed between carbon and oxygen ($p_2 = 1$) and two polar bonds between oxygen and titanium [$p_3 = p_4 = (3 - q_{\text{O}_\mu})/2$] leading to three different principal values $q_{xx} = -q_{210}(7 - q_{\text{O}_\mu})/12; q_{yy} = -q_{210}(1 + 5q_{\text{O}_\mu})/12; q_{zz} = q_{210}(2 + q_{\text{O}_\mu})/3$ with a maximum principal value lying along the z-direction and an asymmetry parameter $\eta_Q = |q_{xx} - q_{yy}|/|q_{zz}| = (3/2)(1 - q_{\text{O}_\mu})/(2 + q_{\text{O}_\mu})$. At last, for the μ_3 -OR case a polar covalent bond was assumed localised between carbon and oxygen ($p_1 = -q_{\text{O}}, a_{1s}^2 = a_{1z}^2 = 1/2, a_{1x}^2 = a_{1y}^2 = 0$) with the three non-bonding MO directed towards the three Ti-atoms: ($p_2 = p_3 = p_4 = 2, a_{2s}^2 = a_{2z}^2 = 1/2, a_{2x} = a_{2y} = a_{3y} = a_{3z} = a_{4x} = a_{4z} = 0, a_{3x} = a_{4y} = 1$) leading to a symmetric efg tensor $q_{xx} = q_{yy} = q_{210}(1 + q_{\text{O}_\mu}/3)/4$ with its maximum principal value lying along the z-direction $q_{zz} = -q_{210}(2 + q_{\text{O}_\mu}/2)$.

Once values have been determined for χ and η_Q , it becomes possible to evaluate the corresponding linewidth in solution at a resonance frequency ω_0 .⁴²

$$\Delta\nu_{1/2} = \frac{3\pi}{20} \times \frac{2I+3}{I^2(2I-1)} \chi^2 \left(1 + \eta_Q^2/3 \right) \times J(\omega_0) \quad (3)$$

In this relation, I stands for the nuclear spin of the quadrupolar nucleus ($I = 5/2$ for the ¹⁷O nucleus), and $J(\omega_0)$ is the reduced spectral density at $\omega = \omega_0$ characterizing molecular reorientation in solution. In the case of rigid spheres of radius a , tumbling in a solution displaying a viscosity η at temperature T , the reduced spectral density may be evaluated as (k_B stands for the Boltzmann constant).⁴²

$$J(\omega) = \frac{2\tau_c}{1 + \omega^2\tau_c^2} \text{ with } \tau_c = \frac{4\pi a^3 \eta}{3k_B T} \quad (4)$$

The molecular radius a was computed from the optimised geometry using standard van der Waals radii: C (170 pm), H (120 pm), O (152 pm).⁴³

Computation of isotropic NMR chemical shifts

On an absolute scale, the isotropic part of the chemical shielding tensor of an NMR-active nucleus submitted to an average excitation energy ΔE and to an electronic population unbalance in p-orbitals P_u is given by:^{32,44}

$$\sigma_{\text{iso}}(\text{ppm}) = \sigma_{\text{dia}}(q) - 966 \times \frac{\langle (a_0/r)^3 \rangle + \kappa q}{\Delta E (\text{eV})} \times P_u \quad (5)$$

The diamagnetic contribution⁴⁵ $\sigma_{\text{dia}}(q)$ was evaluated from Hartree–Fock–Slater wave functions⁴⁶ that also suggest $\kappa \approx 1$ for the effect of partial charge q on the average of the electron–nucleus distance r over valence atomic orbitals of the neutral atoms ($\langle (a_0/r)^3 \rangle_{2p} = 1.23$ and 4.30 a.u. for the ¹³C and ¹⁷O nuclei respectively).⁴⁰ Calling P_{ss} the population of the 2s-orbital and assuming an equal sharing of the total electronic density $P = N - q$ (with N the number of valence electrons) for the other three 2p_x, 2p_y and 2p_z orbitals leads to:³²

$$P_u = \frac{3}{2} \times \left[1 - \left(\frac{q - N + P_{ss} + 3}{3} \right)^2 \right] \quad (6)$$

The average excitation energy ΔE was evaluated by inversion of eqn. (5) using an average isotropic shielding constant $\langle \sigma_{\text{obs}} \rangle$ observed for a set of NMR resonances characterised by the same first coordination sphere and from the corresponding averaged partial charges $\langle q \rangle$ and diamagnetic shifts

$\langle \sigma_{\text{dia}}(q) \rangle$. Values less than 1 eV or much larger than 10 eV usually indicate wrong κ -value or incorrect partial charge distributions. Finally, as far as eqn. (5) is concerned with NMR shielding constants σ and not with chemical shifts δ , all measured chemical shifts have been transformed into their corresponding absolute shielding values. For ^{13}C chemical shifts referenced relative to TMS, the applied transformation was $\sigma(^{13}\text{C})/\text{ppm} = 185.4 - \delta(^{13}\text{C})/\text{ppm}$,⁴⁷ while for ^{17}O chemical shifts referenced relative to tap water, the transformation was $\sigma(^{17}\text{O})/\text{ppm} = 324.0 - \delta(^{17}\text{O})/\text{ppm}$.⁴⁸

Computation of ^1H and ^{13}C T_1 relaxation times

For ^1H nuclei characterized by their magnetogyric ratio γ_{H} and resonating at a frequency ω_0 undergoing intramolecular dipolar interactions at distance r , the contribution to spin-lattice relaxation time was evaluated:⁴²

$$\left(\frac{1}{T_1}\right)_{\text{dd}} = \left(\frac{\mu_0}{4\pi}\right)^2 \times \frac{(\gamma_{\text{H}}^2 \hbar)^2}{20} \times \left(\sum \frac{1}{r^6}\right) \times [12J(2\omega_0) + 3J(\omega_0)] \quad (7)$$

In this relation μ_0 is the vacuum permeability and J the reduced spectral density given by eqn. (4). Generalisation of eqn. (7) for a spin 1/2 nucleus (such as ^1H or ^{13}C) characterized by their magnetogyric ratio γ_{A} and resonating at frequency ω_{A} in dipolar interaction with a nucleus X (spin I , magnetogyric ratio γ_{X} and resonating at frequency ω_{X}) leads to:⁴²

$$\left(\frac{1}{T_1}\right)_{\text{dd}} = \left(\frac{\mu_0 \gamma_{\text{A}} \gamma_{\text{X}} \hbar}{4\pi}\right)^2 \times \frac{I(I+1)}{15} \times \left(\sum \frac{1}{r^6}\right) \times [6J(\omega_{\text{A}} + \omega_{\text{X}}) + 3J(\omega_{\text{A}}) + J(\omega_{\text{A}} - \omega_{\text{X}})] \quad (8)$$

In the case of titanium oxo-alkoxides, the use of eqn. (7) or (8) should be limited to the rigid parts of the molecule that all move with the same correlation time τ_c fixed by the molecular size. For the mobile parts, we also have to consider a local correlation time function of the temperature T that may be written $\tau_c(\text{loc}) = \tau_0 \times \exp(-E_{\text{rot}}/k_{\text{B}}T)$, where k_{B} stands for the Boltzmann constant, τ_0 for the correlation time characterising a free rotation along a given C–H bond and E_{rot} is the activation energy that must be overcome to change the orientation of this C–H bond. This activation energy may be easily evaluated by varying the torsion angle of the considered C–H bond and recording how the total energy (sum of steric, London dispersive and electrostatic energies) is affected by this rotation process.

Results

Acetone is a very convenient solvent allowing one to readily isolate as single-crystals the reaction products between (1) and poly-hydroxylated organic ligands. But, based on our experience of at least 10 different systems, we have noticed that it is imperative to use a co-solvent such as alcohol or 1,4-dioxane in order to get crystals containing the added ligand. If (1) is not diluted in its parent alcohol before reacting with the ligand dissolved in acetone, transparent single crystals are also systematically obtained in large yields but, as shown in Table 1, a wide range of space groups and unit-cell parameters are observed that do not correspond to (2) but rather to

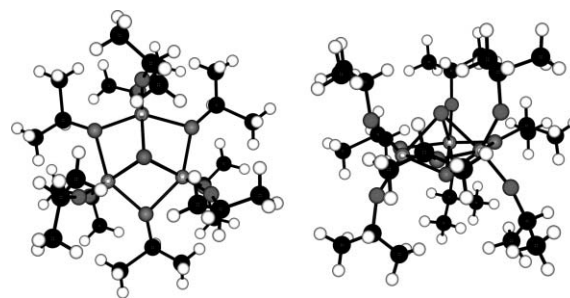


Fig. 2 Molecular structure for (4) found to be present in all crystalline materials gathered in Table 1. Left is a side view of the complex and right is a top view evidencing the basic triangular unit also found in the crystal structure of (2) and in the crystal structure of $[\text{Ti}_3(\mu_3\text{-O})(\mu_3\text{-OR})(\mu\text{-OPr}^i)_3(\text{OPr}^i)_6]$ with $\text{R} = \text{Me}, \text{Pr}^i$.¹² This geometry is characterised by two strongly non-equivalent μ_3 -oxo bridges with $d(\text{Ti}-\text{O}) = 1.972(5) \text{ \AA}$ and $2.203(7) \text{ \AA}$ and $\theta(\text{Ti}-\text{O}-\text{Ti}) = 97.4(3)^\circ$ and $84.5(3)^\circ$ respectively. Bridging OPr^i groups are asymmetric with $d(\text{Ti}-\text{O}) = 1.98(1) \text{ \AA}$ and $2.06(1) \text{ \AA}$, with as expected much shorter Ti–O bonds [$1.784(8) \text{ \AA}$ and $1.798(8) \text{ \AA}$] and rather wide Ti–O–C bond angles [$154.1(6)^\circ$ and $145.8(9)^\circ$ respectively] for terminal OPr^i groups.

$[\text{Ti}_3(\mu_3\text{-O})_2(\mu\text{-OPr}^i)_3(\text{OPr}^i)_6]$. For such a stoichiometry displaying non-equilibrated charges a better formulation would be $[\text{Ti}_3(\mu_3\text{-O})(\mu_3\text{-OH})(\mu\text{-OPr}^i)_3(\text{OPr}^i)_6]$ (4). As R -factors obtained for these non-enolate solutions cannot drop below 10% (the CIF files should be used only for connectivity purposes), it is highly probable that crystallisation involves not only (4) but also a small amount of (2) or (3). These structures were nevertheless quite interesting owing to the absence of disorder among the various isopropoxy groups (Fig. 2). Another rather interesting feature was that after dissolution of the crystals in organic solvents we observed, using natural abundance ^{17}O NMR spectroscopy (Fig. 3b and c), three lines at 565 ppm ($\Delta v_{1/2} = 80 \text{ Hz}$), 558 ppm ($\Delta v_{1/2} < 10 \text{ Hz}$) and 39 ppm ($\Delta v_{1/2} < 10 \text{ Hz}$). As no lines could be observed between 510 and 540 ppm, the formation of $[\text{Ti}_{11}\text{O}_{13}(\text{OPr}^i)_{18}]$ can be ruled out (Fig. 3a). Similarly, the absence of signals near 290 ppm that may be attributed to (1) shows that no molecular rearrangements have occurred after dissolution of the crystals. The absence of signal near 554 ppm that may be attributed to the μ_3 -oxo bridge in (3) and the presence of a line at 39 ppm showing the presence of 2-propanol⁴⁹ suggest that (3) was indeed present in the crystal and was probably hydrolysed by residual water in solution leading to (4) and 2-propanol. The broad signal observed between 562 and 566 ppm, never reported before, could then be tentatively assigned to (2).

The above results point to the rather unusual complexity of crystalline materials isolated when (1) is in contact with acetone. From a previous study,¹² we know that the $^{13}\text{C}\{^1\text{H}\}$ NMR solution spectrum of (3) is characterised by the 4 methine resonances occurring at δ 70.7, 74.7, 76.5 and 78.0 ppm. Concerning the $^{13}\text{C}\{^1\text{H}\}$ NMR solution spectrum of (2), there is an ambiguity because 8 methine resonances were observed instead of 7 according to the crystal structure.¹⁶ In fact, it should be easily understood that owing to its odd number of isopropoxy groups (2) is a key compound for the detailed interpretation of solution NMR spectra of titanium(IV) oxo-alkoxides. Accordingly, with 4 terminal and 3 bridging

Table 1 Observed space group symmetries for transparent and colourless crystalline materials isolated after mixing (1) with either pure acetone or acetone containing a ligand that bears one or several OH groups

Ligand	Space-group	$a/\text{\AA}$	$b/\text{\AA}$	$c/\text{\AA}$	$\alpha/^\circ$	$\beta/^\circ$	$\gamma/^\circ$	Volume/ \AA^3	Reference
Acetone	$P2_1/c$	24.48	14.84	25.67	90	109.3	90	8800	This work
Acetone	$R-3m$	17.89	17.89	21.02	90	90	120	5830	9
Acetone	$R-3m$	12.58	12.58	12.58	91.64	91.64	91.64	1990	10
1,3-Propanediol	$C2/m$	17.4	17.9	12.5	90	92.5	90	3890	This work
Triphenylacetic acid	$R3_2$	17.92	17.92	20.97	90	90	120	5830	This work
2,2'-Biphenol	$R-3$	17.93	17.93	20.99	90	90	120	5850	This work

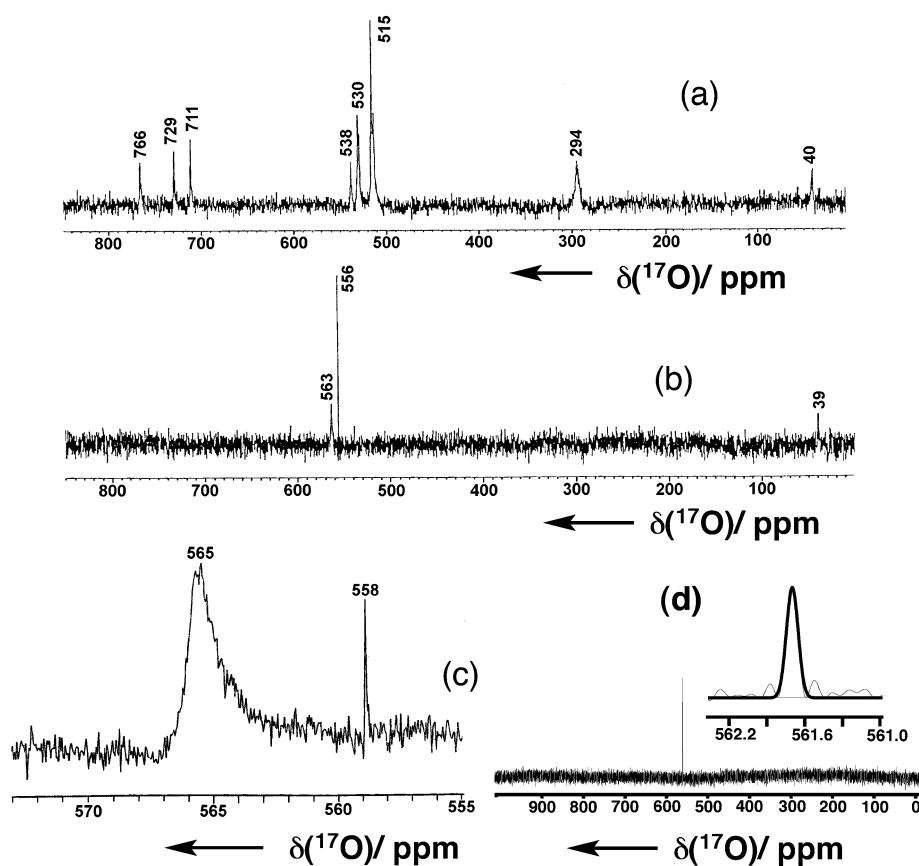
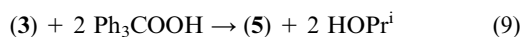
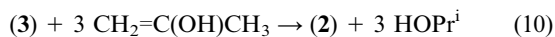


Fig. 3 54.24 MHz ^{17}O NMR spectra of transparent solids dissolved in CDCl_3 after crystallisation from mixtures of (1) with acetone in the absence or presence of a foreign ligand (see Table 1). (a) Evidence for isopropanol (40 ppm), $^{49}\text{Ti}(\text{OPr}^i)_4$ (290 ppm)¹⁴ and $[\text{Ti}_{11}\text{O}_{13}(\text{OPr}^i)_{18}]$ (other peaks)¹³ in the absence of acetone. (b) Crystals with $P2_1/c$ space group obtained using pure acetone. (c) Crystals with $C2/m$ space group obtained with acetone containing 1,3-propanediol. (d) Crystals with probable space group $R-3m$ (checked using ^1H NMR) obtained using a molar ratio 1 : 20 between (1) and pure acetone.

isopropoxy groups, it should be easy, using ^1H NMR spectroscopy, to distinguish after integration between these two kinds of alkoxy groups unambiguously. Then, using 2D NMR techniques such as HSQC and HMBC, this information should be transferred to the ^{13}C NMR solution spectrum, allowing a definitive assignment of bridging relative to terminal resonances. However, the crucial point was to perform such NMR experiments on a non-hydrolysed pure enolate compound (2) not mixed with (3). An elegant solution to this problem was suggested after isolation of the reaction product of (1) with triphenylacetic acid Ph_3COOH in acetone solutions containing 50 vol% of 2-propanol. As shown in Fig. 4, this complex may be formulated $[\text{Ti}_3(\mu_3\text{-O})(\mu\text{-OOPh}_3)_2(\mu\text{-OPr}^i)_3(\text{OPr}^i)_5]$ (5) and may be clearly viewed as the result of a selective reaction between the triphenylacetic acid molecule and the ($\mu_3\text{-OPr}^i$) site of (3):



The above reaction is in fact in competition with the selective substitution of the ($\mu_3\text{-OPr}^i$) site by the enol form of acetone followed by the aldol condensation of two other acetone molecules on the $[\text{Ti}_3(\mu_3\text{-O})(\mu\text{-OPr}^i)_3]$ core acting as a templating agent:



As evidenced by reactions (9) and (10), dissolving triphenylacetic acid in pure acetone should favour the formation of (2) and (5) and insure the complete consumption of (3). Now, owing to the quite different molecular sizes of (2) and (5), there is very little chance that they would co-crystallise and one may expect to get crystals of (2) completely free from (3) or (5).

Fig. 5 shows the $^{13}\text{C}\{^1\text{H}\}$ NMR solution spectrum of such crystals obtained after mixing (1) with triphenylacetic acid dissolved in pure acetone. As expected, the major product is (2) owing to the occurrence of seven strong methine resonances between 70 and 80 ppm (Table 2) mixed with a very small

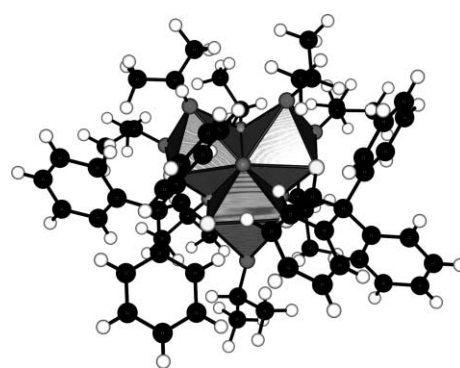


Fig. 4 Molecular structure for $[\text{Ti}_3(\mu_3\text{-O})(\mu\text{-OOPh}_3)_2(\mu\text{-OPr}^i)_3(\text{OPr}^i)_5]$ (5) that may be viewed as the reaction product between $[\text{Ti}_3(\mu_3\text{-O})(\mu_3\text{-OPr}^i)(\mu\text{-OPr}^i)_3(\text{OPr}^i)_6]$ (3) and triphenylacetic acid after selective substitution of one $\mu_3\text{-OPr}^i$ bridging and one terminal isopropoxy group. Owing to the steric crowding imposed by the rather bulky triphenylacetate ligand, the $\mu_3\text{-oxo}$ bridges are asymmetric with $d(\text{Ti}-\text{O}) = 1.93\text{--}2.00 \text{ \AA}$ and $\theta(\text{Ti}-\text{O}-\text{Ti}) = 104\text{--}106^\circ$. For bridging OPr^i groups, two of them are found to be strongly asymmetric with $d(\text{Ti}-\text{O}) = 1.92\text{--}1.94 \text{ \AA}$ on one side and $d(\text{Ti}-\text{O}) = 2.14\text{--}2.20 \text{ \AA}$ on the other side, the last one being nearly symmetric with $d(\text{Ti}-\text{O}) = 2.01$ and 2.03 \AA on each side. Terminal OPr^i groups are as expected characterised by short $\text{Ti}-\text{O}$ bonds ($1.77\text{--}1.82 \text{ \AA}$) and rather wide $\text{Ti}-\text{O}-\text{C}$ bond angles ($139\text{--}162^\circ$). Bridges involving the carboxylate moiety are found to be almost perfectly symmetric (2.09 \AA on both sides for each ligand) with a rather open $\text{O}-\text{C}-\text{O}$ bond angle (125°).

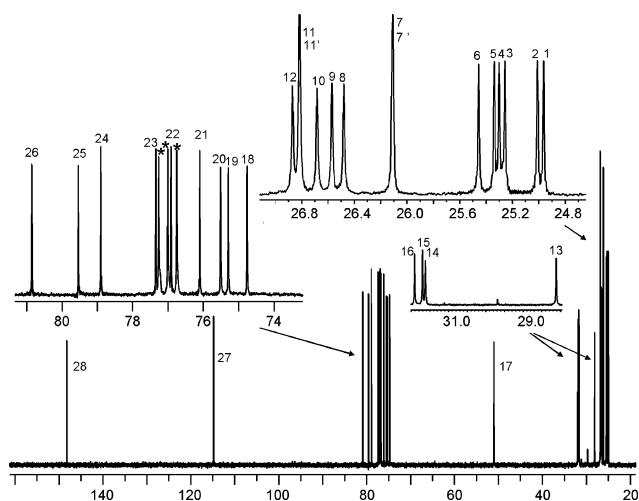


Fig. 5 125.7 MHz $^{13}\text{C}\{^1\text{H}\}$ NMR solution spectrum ($T = 273\text{ K}$) obtained after dissolution in CDCl_3 of crystals isolated after mixing (1) with pure acetone containing triphenylacetic acid. NMR signals have been arbitrarily labelled from right to left for further identification.

amount of (5). From a comparison with the previously published NMR data on (2),¹⁶ it may be concluded that the resonance observed at 79.7 ppm does not belong to (2). Fig. 6 shows the ^1H NMR spectrum recorded at 500 MHz after dissolution of crystals of (2) in CDCl_3 . Between 4.0 and 5.0 ppm we observe seven septuplets that may be easily separated after integration in two groups, the first one integrating for 4 protons above 4.6 ppm and the second one integrating for 3 protons below 4.6 ppm. Exactly the same grouping is observed in the methyl region with 8 doublets below 1.3 ppm and 6 doublets above 1.3 ppm. Other observed signals correspond either to acetone or to the enolate ligand in agreement with previously published NMR data.¹⁶

Table 2 Partial assignment of the ^1H and $^{13}\text{C}\{^1\text{H}\}$ NMR spectra of solutions of (2) in CDCl_3 after recording of 2D HSQC and HMBC NMR spectra. (sg) stands for singlet, (d) for doublet and (sp) for septuplet

^1H -signal	$\delta(^1\text{H})/\text{ppm}$	^{13}C -signal	$\delta(^{13}\text{C})/\text{ppm}$	Assignment	C–C bonding
1	1.185 (d)	1	24.96	Ti–OCH(CH ₃) ₂	24
2	1.196 (d)	7	26.10	Ti–OCH(CH ₃) ₂	21
3	1.200 (d)	2	25.00	Ti–OCH(CH ₃) ₂	24
4	1.210 (d)	7'	26.10	Ti–OCH(CH ₃) ₂	21
5	1.212 (sg)	16	31.90	Ti–OC(C)(CH ₃) ₂	25
6	1.216 (sg)	13	28.11	Ti–OC(C)(CH ₃) ₂	26
7	1.230 (sg)	15	31.69	Ti–OC(C)(CH ₃) ₂	26
8	1.240 (d)	3	25.25	Ti–OCH(CH ₃) ₂	22 or 23
9	1.240 (d)	4	25.30	Ti–OCH(CH ₃) ₂	22 or 23
10	1.240 (d)	5	25.33	Ti–OCH(CH ₃) ₂	22 or 23
11	1.269 (d)	6	25.45	Ti–OCH(CH ₃) ₂	22
12	1.316 (sg)	14	25.45	Ti–OC(C)(CH ₃) ₂	25
13	1.360 (d)	9	26.57	Ti ₂ –OCH(CH ₃) ₂	20
14	1.380 (d)	10	26.68	Ti ₂ –OCH(CH ₃) ₂	20
15	1.420 (d)	12	26.87	Ti ₂ –OCH(CH ₃) ₂	19
16	1.460 (d)	11	26.81	Ti ₂ –OCH(CH ₃) ₂	18
17	1.470 (d)	11'	26.81	Ti ₂ –OCH(CH ₃) ₂	18
18	1.473 (d)	8	26.47	Ti ₂ –OCH(CH ₃) ₂	19
19	2.070 (d)	17	50.91	CH ₂ (CO) ₂	26, 28
20	2.168 (sg)	—	—	CH ₃ C=O	—
21	2.480 (d)	17	50.91	CH ₂ (CO) ₂	26, 28
22	4.452 (sg)	27	114.81	(O)C–CH=C(O)	25, 28
23	4.474 (sp)	20	75.50	Ti ₂ –OCH(CH ₃) ₂	9, 10
24	4.530 (sp)	19	75.28	Ti ₂ –OCH(CH ₃) ₂	8, 12
25	4.567 (sp)	18	74.75	Ti ₂ –OCH(CH ₃) ₂	11
26	4.703 (sp)	21	76.09	Ti–OCH(CH ₃) ₂	7
27	4.781 (sp)	22	76.90	Ti–OCH(CH ₃) ₂	6, (3, 4, 5)
28	4.800 (sp)	23	77.33	Ti–OCH(CH ₃) ₂	(3, 4, 5)
29	4.900 (sp)	24	78.89	Ti–OCH(CH ₃) ₂	1, 2
—	—	25	79.53	C=CH–C(O)Me ₂	14, 16, 27
—	—	26	80.85	CH ₂ –C(O)Me ₂	13, 15, 17
—	—	28	148.12	COTi ₃	17, 27

In order to confirm this assignment, we have also measured both ^{13}C and ^1H T_1 relaxation times as it is usually assumed from the literature that a bridging position should be associated with shorter T_1 -values.⁵⁰ As shown in Table 3, this was found to be the case for ^{13}C methine resonances as the mean value for signals C18–C20 was 1.66 s (bridges) vs. 1.82 s for signals C21–C24 (terminal groups). Similarly, for ^1H methine resonances the mean value for signals H23–H25 was 1.31 s (bridges) vs. 1.57 s for signals H26–H29 (terminal groups).

After this clear discrimination between terminal and bridging isopropoxy groups, a full assignment within these two classes, each spanning a very tiny 5 ppm range is still wanted. Relying on 2D-techniques, the HSQC NMR spectra of (2) were first recorded at 500 MHz in CDCl_3 (Fig. 7) in order to identify unambiguously each C–H bond through a pair of ^{13}C and ^1H signals. Then recording the HMBC NMR spectra under similar conditions (Fig. 8), allows the observed resonances to be classified as four terminal isopropoxy groups, three bridging isopropoxy groups and one μ_3 -enolate group.

At this stage, it was possible to make some tentative assignments about which is which among the 4 terminal OPrⁱ resonances. Referring to Fig. 9 a pseudo symmetry plane may be defined involving the Ti-atom bearing two terminal isopropoxy groups, the μ_3 -oxo bridge, the μ_3 -enolate bridge, and the μ -OPrⁱ group bridging the two Ti-atoms bearing a single isopropoxy group. In the following, the label 'm' will refer to atoms lying on this pseudo symmetry plane. For atoms lying outside this plane, the label '=' will refer to a region lying on the same side as the C=C double bond, whereas the label 'x' will refer to the opposite region lying on the same side as the methylene group. Finally, the symbol '+' will be used for the region above the plane defined by the three μ -OPrⁱ group containing the enolate ligand, whereas for the opposite region containing the μ_3 -oxo group, we will use the '-' minus symbol. With this convention, the eight NMR signals arising from

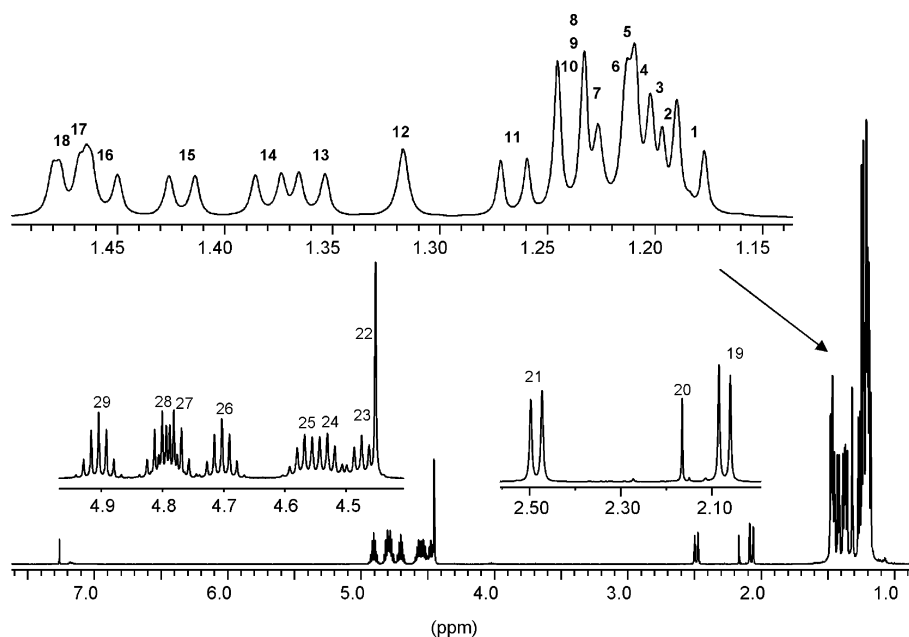


Fig. 6 500 MHz ^1H NMR solution spectrum ($T = 273$ K) obtained after dissolution in CDCl_3 of crystals isolated after mixing (**1**) with pure acetone containing triphenylacetic acid. NMR signals have been arbitrarily labelled from right to left for further identification.

terminal isopropoxy groups may be labelled: $\underline{\text{CHm}}$ +, $\underline{\text{CHm}}$ +, $\underline{\text{CHm}}$ -, $\underline{\text{CHm}}$ -, $\underline{\text{CHx}}$, $\underline{\text{CHx}}$, $\underline{\text{CH=}}$ and $\underline{\text{CH=}}$, the bold and underlined letters referring to the corresponding ^1H or $^{13}\text{C}\{^1\text{H}\}$ NMR peaks. A first association ($\text{H27, H28} \leftrightarrow \underline{\text{CHx}}, \underline{\text{CH=}}$) is strongly suggested as these two terminal OPr^i groups differ only in their position relative to the double bond which explains their very similar chemical shifts. Combination of this information with the integration of the ^1H spectrum then leads to the second association ($\text{H26, H29} \leftrightarrow \underline{\text{CHm}}$ +, $\underline{\text{CHm}}$ -), and from Table 2 we should have ($\text{C22, C23} \leftrightarrow \underline{\text{CHx}}, \underline{\text{CH=}}$) and ($\text{C21, C24} \leftrightarrow \underline{\text{CHm}}$ +, $\underline{\text{CHm}}$ -) on one hand and between $\underline{\text{CHm}}$ +, $\underline{\text{CHm}}$ - on the other hand is thus clearly associated with the fact that $\underline{\text{CHm}}$ + and $\underline{\text{CHm}}$ + are facing an

Table 3 ^1H and ^{13}C room temperature spin lattice relaxation times for solutions of (**2**) in CDCl_3 . T_1 -value was not measured for C22 owing to overlapping with CDCl_3 resonances. The large error for signals H1 to H11 comes from the fact that all these resonances were treated as a single block for integration

^{13}C -signal	T_1/s	^1H -signal	T_1/s	Assignment
1, 2	1.05 (5)	1, 3	2(2)	$\text{Ti-OCH}(\underline{\text{CH}}_3)_2$
3-6	1.63 (3)	8-11	2(2)	$\text{Ti-OCH}(\underline{\text{CH}}_3)_2$
7	1.24 (3)	2, 4	2(2)	$\text{Ti-OCH}(\underline{\text{CH}}_3)_2$
8	1.15 (3)	18	0.78(4)	$\text{Ti}_2\text{-OCH}(\underline{\text{CH}}_3)_2$
9, 10	1.15 (3)	13, 14	0.91(6)	$\text{Ti}_2\text{-OCH}(\underline{\text{CH}}_3)_2$
11	1.16 (2)	16, 17	0.78(4)	$\text{Ti}_2\text{-OCH}(\underline{\text{CH}}_3)_2$
12	1.16 (3)	15	0.82(5)	$\text{Ti}_2\text{-OCH}(\underline{\text{CH}}_3)_2$
13	0.56 (3)	6	2(2)	$\text{Ti-OC}(\underline{\text{C}})(\underline{\text{CH}}_3)_2$
14	0.54 (3)	12	0.5(2)	$\text{Ti-OC}(\underline{\text{C}})(\underline{\text{CH}}_3)_2$
15	0.54 (3)	7	2(2)	$\text{Ti-OC}(\underline{\text{C}})(\underline{\text{CH}}_3)_2$
16	0.49 (2)	5	2(2)	$\text{Ti-OC}(\underline{\text{C}})(\underline{\text{CH}}_3)_2$
17	0.44 (1)	19	0.453(2)	$\underline{\text{CH}}_2(\underline{\text{CO}})_2$
17	0.44 (1)	21	0.440(4)	$\underline{\text{CH}}_2(\underline{\text{CO}})_2$
18	1.70 (5)	25	1.32(7)	$\text{Ti}_2\text{-OCH}(\underline{\text{CH}}_3)_2$
19	1.67 (5)	24	1.32(7)	$\text{Ti}_2\text{-OCH}(\underline{\text{CH}}_3)_2$
20	1.61 (4)	23	1.29(6)	$\text{Ti}_2\text{-OCH}(\underline{\text{CH}}_3)_2$
21	1.85 (7)	26	1.58(2)	$\text{Ti-OCH}(\underline{\text{CH}}_3)_2$
22	—	27	1.59(4)	$\text{Ti-OCH}(\underline{\text{CH}}_3)_2$
23	1.84 (6)	28	1.59(4)	$\text{Ti-OCH}(\underline{\text{CH}}_3)_2$
24	1.76 (5)	29	1.53(3)	$\text{Ti-OCH}(\underline{\text{CH}}_3)_2$
25	>6	—	—	$\text{C=CH-C}(\underline{\text{O}})\text{Me}_2$
26	>6	—	—	$\text{CH}_2\text{-C}(\underline{\text{O}})\text{Me}_2$
27	0.9(1)	22	1.29(6)	$(\underline{\text{O}})\text{C-CH=C}(\underline{\text{O}})$
28	>6	—	—	$\underline{\text{COT}}_3$

enolate group whereas $\underline{\text{CHm}}$ - and $\underline{\text{CHm}}$ - are facing a μ_3 -oxo group. By the same kind of reasoning, we expect a clear separation between ($\text{H23} \leftrightarrow \underline{\mu\text{CHm}}$) and the pair ($\text{H24, H25} \leftrightarrow (\underline{\mu\text{CHx}}, \underline{\mu\text{CH=}})$), leading after Table 2 to the association ($\text{C20} \leftrightarrow \underline{\mu\text{CHm}}$) and ($\text{C18, C19} \leftrightarrow (\underline{\mu\text{CHx}}, \underline{\mu\text{CH=}})$). However from Table 2 we may also notice that the *gem*-methyl groups borne by the C18–H25 pair have the same ^{13}C resonance in deep contrast with the two other pairs C19–H24 and C20–H23 that are characterised by two resolved ^{13}C peaks for their respective *gem*-methyl groups. Now from the dihedral angles involving the C=C double bond on one hand and the three $\mu\text{O-C}$ bonds on the other hand, we expect three different values: 180° ($\underline{\mu\text{COx}}$), $+60^\circ$ ($\underline{\mu\text{COM}}$) and -60° ($\underline{\mu\text{CO=}}$). Linking the most symmetrical environment relative to the C=C double bond for the *gem*-methyl groups to the 180° value, suggests the assignments ($\text{H25} \leftrightarrow \underline{\mu\text{CHx}}$) and ($\text{H24} \leftrightarrow \underline{\mu\text{CH=}}$). From Table 2, it thus follows that we should have ($\text{C18} \leftrightarrow \underline{\mu\text{CHx}}$) and ($\text{C19} \leftrightarrow \underline{\mu\text{CH=}}$).

As the above analysis based on HSQC and HMBC data allows only a partial assignment of the ^1H or $^{13}\text{C}\{^1\text{H}\}$ NMR spectra, we have also recorded the COSY and ROESY NMR spectra of (**2**) at 500 MHz. With the ROESY technique (Fig. 10), it was possible to detect, using a single NMR experiment, protons undergoing chemical exchange as well as protons that are coupled through dipolar interactions owing to their close proximity in space. The COSY spectrum was recorded (Fig. 11) in order to be able to identify residual COSY correlations in the ROESY spectrum. First, we may notice the presence in the COSY and ROESY spectra of exchange correlations involving free isopropanol. Fortunately, under a higher magnification, it was observed that these correlations do not concern (**2**) but rather an impurity in quite low concentration, identified as (**5**). From this very informative ROESY spectrum we were able to build Table 4 giving the assignment for all ^1H resonances with the exception of five methyl groups (signals 1, 3, 8, 9 and 10) that are too close in chemical shift to be distinguished. As a consistency check, we may have a look at the exchange domain of the ROESY spectrum (bottom right in Fig. 11) showing that: ($\text{H23} \leftrightarrow \text{H27,28}$), ($\text{H24} \leftrightarrow \text{H27,29}$), ($\text{H25} \leftrightarrow \text{H28,28}$) and ($\text{H26} \leftrightarrow \text{H29}$). Referring to Table 4 and Figure 9, this means that chemical exchange between bridging and terminal positions occurs only on the μ_3 -oxo side, involving two terminal isopropoxy groups

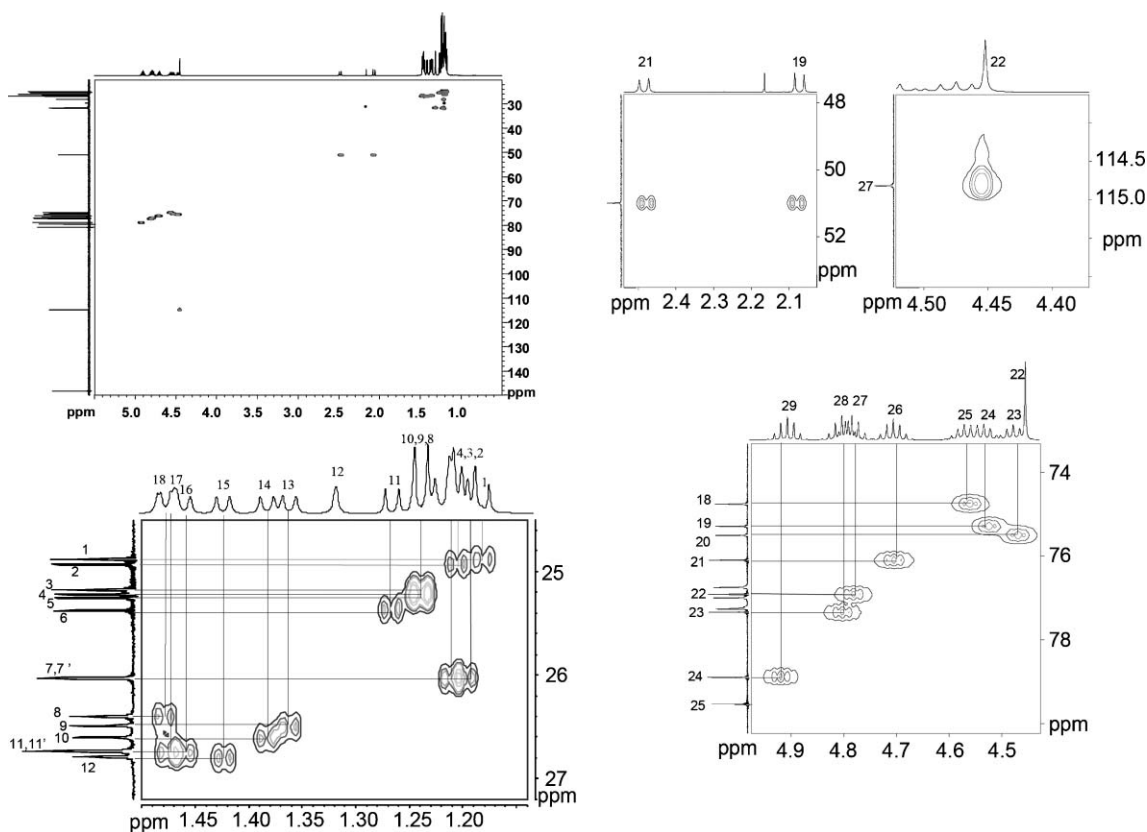


Fig. 7 HSQC 2D NMR solution spectrum ($T = 273$ K) obtained after dissolution in CDCl_3 of crystals isolated after mixing (1) with pure acetone containing triphenylacetic acid. This pulse sequence relates ^1H signals (top) and ^{13}C signals (left) characterised by the existence of a scalar $^1J_{\text{C-H}}$ coupling constant (*i.e.* corresponding to C–H chemical bonds).

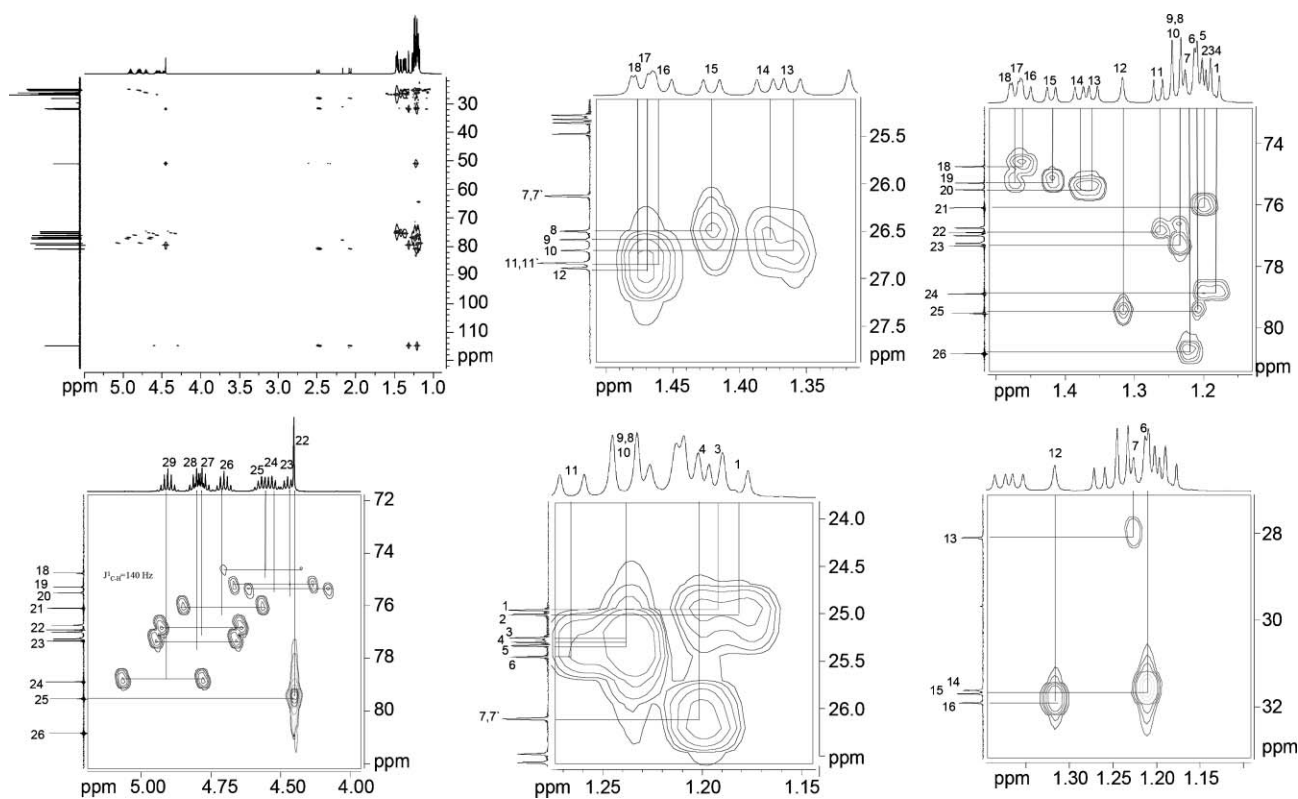


Fig. 8 HMBC 2D NMR solution spectrum ($T = 273$ K) obtained after dissolution in CDCl_3 of crystals isolated after mixing (1) with pure acetone containing triphenylacetic acid. This pulse sequence relates ^1H signals (top) and ^{13}C signals (left) characterised by the existence of scalar $^2J_{\text{C-H}}$ and $^3J_{\text{C-H}}$ H,C correlations (*i.e.* corresponding to one or two C–C chemical bonds).

lying in *cis*-positions relative to a given bridging ligand. As expected on steric grounds, the only exchange process involving the upper part of the complex (enolate region)

occurs between Om+ and Om– located on the same Tim site, bringing a strong support for the validity of the proposed assignment.

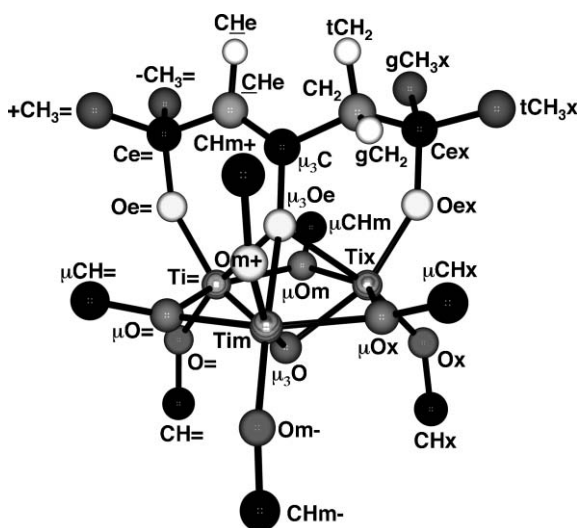


Fig. 9 Geometry and labelling of the rigid core of (2) according to single-crystal X-ray diffraction data. Label 'm' refers to the existence of a pseudo symmetry plane, 'm+' and 'm-' referring to atoms lying on the $\mu_3\text{Oe}$ or $\mu_3\text{O}$ sides respectively. Label 'x' indicates atoms lying on the methylene CH_2 side, whereas label '=' is given to atoms lying on the methine $=\text{CH}$ side. For the two *gem*-di-methyl pairs of the μ_3 -enolate ligand, label '+' is added to atoms lying on the $\text{Om}+$ side whereas label '-' is given to atoms lying in the opposite direction (*i.e.* on the μCHm side).

Discussion

The above results have shown how it was possible to get a full experimental assignment of the ^1H and ^{13}C NMR spectrum of (2) providing a firm basis for testing the ability of theoretical models to correlate observed positions of NMR peaks or measured relaxation times with molecular structure. Fig. 12 (right) shows the molecular structure obtained after optimisation of (2) in the vacuum at $T = 0\text{ K}$, a situation quite different from the experimental one referring to a complex tumbling in chloroform at room temperature. By comparison, Fig. 12 (left) shows the final geometry after embedding of the complex within its crystalline lattice. In order to decide which structure

is closest from the experimental one, we may refer to Fig. 11 (top left) showing that H21 lies in close proximity of both H25 (μCHx site) and H26 ($\text{CHm}+$ site) with the shortest distance being between H21 and H25 (more intense correlation). Referring to the vacuum-optimised structure we found that $d(\text{H21-H25}) = 2.35\text{ \AA}$ vs. $d(\text{H21-H26}) = 2.27\text{ \AA}$ in poor agreement with experiments. On the other hand for the $R-3m$ constrained structure we found $d(\text{H21-H25}) = 2.39\text{ \AA}$ vs. $d(\text{H21-H26}) = 2.43\text{ \AA}$ in better coherence with experimental data. Another independent way is to look at the total steric repulsive energy of the two models that was found to be $+103.772\text{ kJ mol}^{-1}$ for the vacuum case and $+103.307\text{ kJ mol}^{-1}$ for the crystalline case. It may then be concluded that owing to the higher number of optimised angles, the vacuum-state structure has landed into a deep false minimum that was not explored in the solid-state optimisation. Consequently, we have selected the $R-3m$ structure (Fig. 12, left) that is in better agreement with experiments for this discussion.

Let's first consider the partial charge distribution on heavy atoms (Table 5). At one extreme lies the μ_3 -oxo site (strong negative charge), while at the other extreme the three Ti-atoms (strong positive charge) are found. Concerning the non-methyl C-atoms we found, in the order of decreasing charges, the CC_3O site of the enolate ligand near the methylene group, the CC_3O site of the enolate ligand near the methine group, a set gathering the 4 methine moieties of terminal isopropoxy groups, a set made of the 3 methine moieties of bridging isopropoxy groups, the CC_2O site of the enolate ligand, the methine CC_2H site and the methylene group. With the exception of the two double bonded C-atoms (well-known deshielding effect on the $\text{C}=\text{C}$ double bond), this is just the order of decreasing chemical shifts, a very satisfying result. For methyl groups, we observed in agreement with NMR experiments that the *gem*-di-methyl groups of the enolate ligand are on average less negative than the *gem*-di-methyl groups of the isopropoxy groups. A notable exception is the mixing observed between *gem*-di-methyl groups of the terminal isopropoxy group facing the enolate group and the *gem*-di-methyl groups of the enolate ligand. In fact, this should not be very surprising as, owing to chemical exchange, chemical shifts of terminal groups were found to be strongly temperature dependent. It

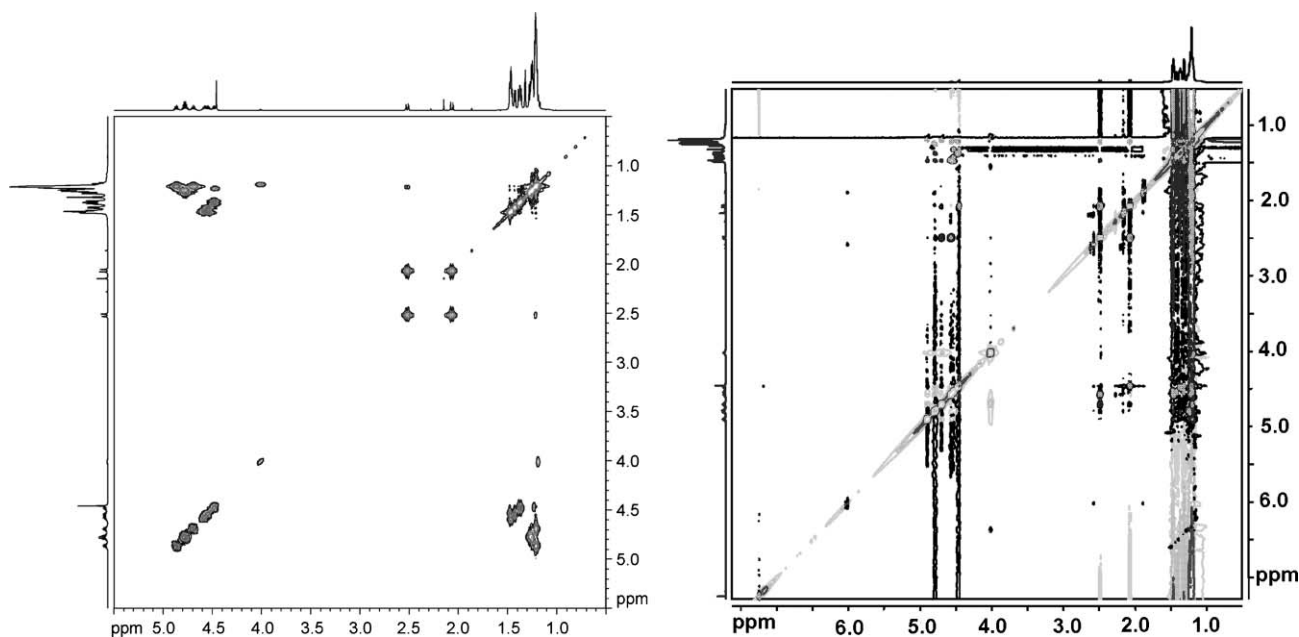


Fig. 10 COSY (left) and ROESY (right) 2D NMR solution spectrum ($T = 273\text{ K}$) obtained after dissolution in CDCl_3 of crystals isolated after mixing (1) with pure acetone containing triphenylacetic acid. The ROESY pulse sequence relates ^1H signals (top and left) characterised by the existence of dipolar H,H correlations owing to a close proximity in space (black) or H-atoms in chemical exchange (light grey). The COSY spectrum was recorded to identify residual COSY peaks in the ROESY spectrum.

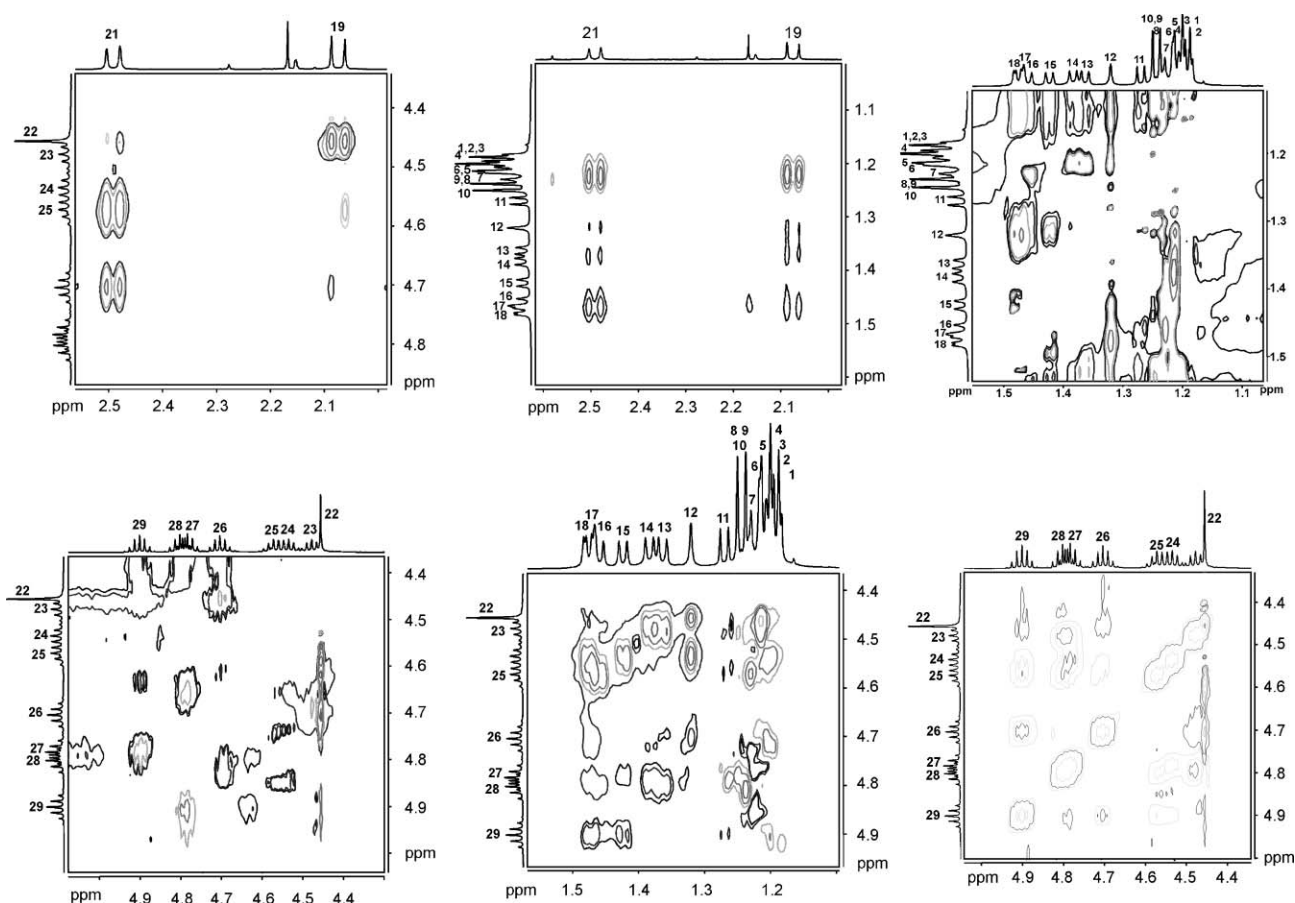


Fig. 11 Details for the ROESY spectrum displayed in Fig. 10 from which Table 4 were deduced. Top left: dipolar methylene-methine correlations, top middle: methylene-methyl dipolar correlations, bottom left: methine-methine dipolar correlations, bottom middle: methine-methyl dipolar correlations, top right: methyl-methyl dipolar correlations, bottom right: methine-methine exchange correlations.

thus emerges that the partial charge distribution given in Table 5 gives the same overall picture as the $^{13}\text{C}\{^1\text{H}\}$ NMR spectrum. As expected, by looking at details this naïve picture breaks down, but it nevertheless remains that, at a purely

qualitative level, our atomic charges are what we would expect in view of the $^{13}\text{C}\{^1\text{H}\}$ NMR spectrum. For a more quantitative test of the validity of these charges we may rely on relations (5) and (6). Let's for instance focus on the 5 ppm

Table 4 Definitive assignment of the ^1H and $^{13}\text{C}\{^1\text{H}\}$ NMR spectra of solutions of (2) in CDCl_3 after recording of 2D ROESY NMR spectrum. See Fig. 9 for the meaning of the labels. For *gem*-di-methyl groups belonging to isopropoxy groups (not represented in Fig. 9) and that may be assigned from the ROESY spectrum (signals 2, 4, 15, 16, 17, 18 and 11), we use a label '+' to refer to a methyl group lying near the pseudo mirror plane (defined by Om^- , Tim , Om^+), the label '-' being given to the other partner

^1H -peak	#1	#2	#3	#4	#5	#6	Assignment
1,3	29	—	—	—	—	—	$-\text{CH}(\text{CH}_3)_2$
2	22	24	26	—	—	—	$=\text{CH}_3\text{m}^+$
4	21	25	26	29	—	—	xCH_3m^+
5	12	13	22	23	—	—	$-\text{CH}_3 =$
6	14	19	21	23	—	—	$-\text{CH}_3\text{x}$
7	16	19	21	25	—	—	$+\text{CH}_3\text{x}$
8,9,10	12	15	23	27	28	—	$-\text{CH}(\text{CH}_3)_2$
11	12	27	29	—	—	—	$+\text{Me} =$
12	5,8,9,10	11,15,18	19,21	22	24	26	$+\text{CH}_3 =$
13	5	23	27	—	—	—	$=\mu\text{CH}_3\text{m}$
14	6	19,21	23	28	—	—	$\text{x}\mu\text{CH}_3\text{m}$
15	8,9,10	12	24	27	29	—	$+\mu\text{CH}_3 =$
16	7	19	25	28	—	—	$-\mu\text{CH}_3\text{x}$
17	21	25	26	—	—	—	$+\mu\text{CH}_3\text{x}$
18	12	24	26	—	—	—	$-\mu\text{CH}_3 =$
19	6	7	12	14	16	22,26	tCH_2
21	4	6	7,12	14,17	22,25	26	gCH_2
22	5	12	19	21	24	26	CHe
23	5	6	8,9,10	13	14	26	μCHm
24	2	12	15	18	22	—	$\mu\text{CH} =$
25	4	7	16	17	21	—	μCHx
26	4	12	17	18	19,21	22,26	CHm^+
27	8,9,10	11	13	15	29	—	$\text{CH} =$
28	8,9,10	14	16	29	—	—	CHx
29	1,3	4	11	15	27	28	CHm^-

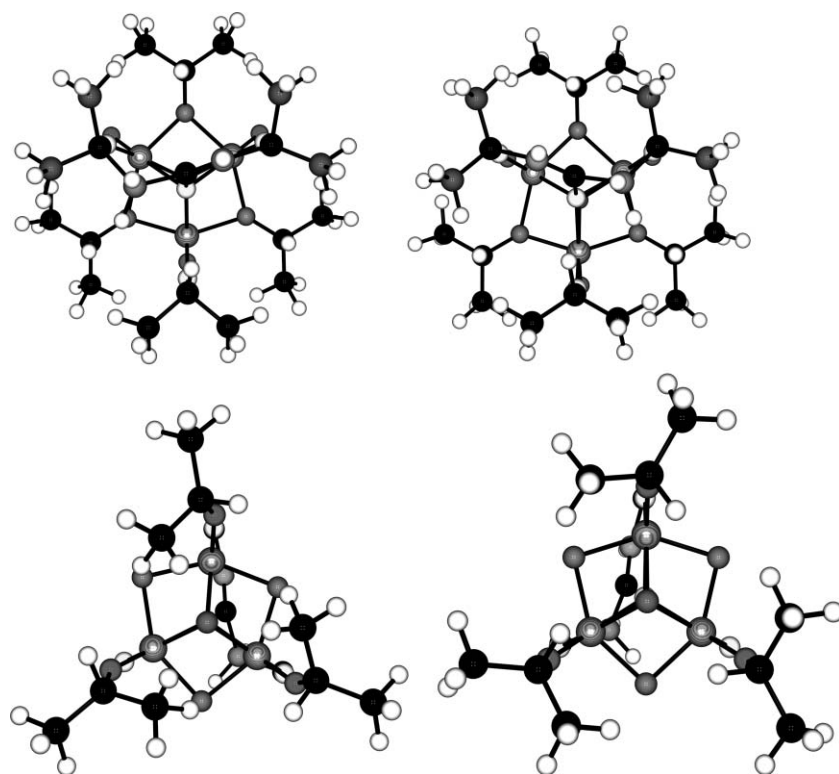


Fig. 12 Two optimised theoretical models for the molecular structure of (2) according to the PACHA algorithm. Left: top view (enolate at the front) and bottom view (enolate at the bottom) for the solid-state optimisation constrained by the $R-3m$ space group. Right: top view (enolate at the front) and bottom view (enolate at the bottom) for the vacuum unconstrained optimisation. Owing to the lack of a pseudo C_3 -symmetry axis in the molecular case (right) the steric compression energy was found to be much higher (about 470 kJ mol^{-1}) than in the solid-state case (left).

range spanned by the 7 methine resonances of isopropoxy groups. As shown in Table 5 this corresponds to a partial charge variation $\Delta q \approx 0.03$. From the knowledge of the chemical shift barycentre $\langle \delta \rangle = 76.32 \text{ ppm}$, we computed from relation (5) assuming that $P_{ss} \approx 1$ an average excitation energy $\Delta E = 10.2 \text{ eV}$ well in line with the fact that we are dealing with sp^3 C-atoms. On this basis, (5) predicts that, on average, the expected difference in chemical shifts between bridging and terminal position should be -3.2 ppm to be compared with the experimental -2.1 ppm value. The same procedure applied to the corresponding 14 methyl groups leads to a slightly higher average excitation energy $\Delta E = 12.9 \text{ eV}$ (no oxygen atoms in the first coordination sphere) and leads to a predicted chemical shift range of $\Delta\delta_{th} = 1.7 \text{ ppm}$ ($\Delta q \approx 0.01$) that compares pretty well with the observed experimental $\Delta\delta_{exp} = 1.9 \text{ ppm}$ value. It is worth noting that, at this level of charge variation and chemical shift range, we may encounter big trouble by trying a direct comparison between experimental and calculated chemical shifts. Accordingly, for a 2 ppm chemical shift range we are entering a zone where solvent and temperature effects are not negligible, whereas for a partial charge range of about 0.01 we are running into ellipsoids of vibration for X-ray diffraction and the problem of occurrence of false minima for optimised structures. Consequently, we will not consider for such highly resolved NMR spectra absolute chemical shifts values, but limit ourselves to chemical shift ranges. A further test may concern the $+1.3 \text{ ppm}$ difference observed between sites \underline{C}_{ex} and $\underline{C}_{e=}$. As seen from Table 5, PACHA correctly predicts that the more shielded signal should be $\underline{C}_{e=}$, but from (5) it is deduced that $\Delta E = 10.3 \text{ eV}$ and $\Delta\delta_{th} = 0.04 \text{ ppm}$ ($\Delta q \approx 0.0002$) which is clearly too small to explaining the experimental value. Similarly, for the four *gem*-di-methyl groups of the enolate ligands it is found that $\Delta E = 12.4 \text{ eV}$ and $\Delta\delta_{th} = 0.2 \text{ ppm}$ ($\Delta q \approx \sim 0.002$) to be compared with $\Delta\delta_{exp} = 3.8 \text{ ppm}$. Here it is clear that such a difference in chemical shift cannot be attributed to the paramagnetic term and should then arise from the diamagnetic

term (presence of a $\underline{C}=\underline{C}$ double bond for $\underline{C}_{e=}$ and of a methylene group for \underline{C}_{ex}). Considering the last two as yet uninvestigated C-atoms defining the $\underline{C}=\underline{C}$ double bond ($\mu_3\underline{C}$ and \underline{C}_{He}), the observed 33 ppm difference should be attributed to a difference in ΔE -values (7.0 eV for the $\underline{C}\underline{C}_2\underline{O}$ site against 7.8 eV for the $\underline{C}\underline{C}_2\underline{H}$ site) rather than to a difference in electronic density ($\Delta q \approx 0.056$) that would correspond to at most 20 ppm.

Concerning ^{17}O NMR chemical shifts and assuming $P_{ss} \approx 2$ (lone pair for the low-lying s-orbital), it comes from the experimental 562 ppm value that $\Delta E = 4.7 \text{ eV}$. Referring to the band structure of the anatase polymorph ($E_g \approx 3.3 \text{ eV}$ with valence band width of about $\Delta \approx 4 \text{ eV}$)¹ that displays very similar μ_3 -oxo groups, it may be expected for a molecular species $\Delta E \approx E_g + \Delta/2 \approx 5.3 \text{ eV}$ in good agreement with the above value derived from the knowledge of the partial charge and of the ^{17}O NMR chemical shift. Concerning nuclear quadrupole coupling constants, Table 6 shows what is expected for this oblate-shaped molecule characterised by a molecular volume $V = 660 \text{ \AA}^3$, $R_{max} = 8.0 \text{ \AA}$ (largest linear dimension) and $\langle R \rangle = 5.4 \text{ \AA}$, radius of the equivalent sphere such that $(4/3)\pi \langle R \rangle^3 = V$.⁵¹ In both cases, in agreement with experiments, it is found that under extreme narrowing conditions [$J(\omega) \approx \tau_c$], only the μ_3 -oxo group should be detected under standard conditions. One may also notice the quite low linewidth predicted for this μ_3 -oxo bridge assuming $\gamma_\infty = 0$. However, the experimentally observed value $\Delta\nu_{1/2} = 11 \text{ Hz}$ may be easily recovered if a Sternheimer antishielding factor of $|1 - \gamma_\infty| = 1.9$ or 3.3 is used for R_{max} and $\langle R \rangle$ respectively. The 3.3 value being very close to the value (3.1) derived from the rutile structure¹ that contains also μ_3 -oxo bridges, $\langle R \rangle$ seems to be a better estimator for the rotational correlation time τ_c than R_{max} .

A more convincing way of checking this point is to rely on the measured T_1 -values for a rigid site in the molecule. A good candidate is the methine group belonging to the enolate double bond. Using the R_{max} -value and assuming a 1.08 \AA C-H bond

Table 5 Partial charge distribution for the structural model of (2) shown in Fig. 12 (left)

Atomic site	Partial charge q	^1H signal	^{13}C signal
$\mu_3\text{O}$	-0.84858	—	—
Oe	-0.67329	—	—
$\mu\text{O}=\text{}$	-0.64046	—	—
μOx	-0.64041	—	—
μOm	-0.64005	—	—
Ox	-0.55105	—	—
O=	-0.55102	—	—
Om-	-0.55000	—	—
Om+	-0.53994	—	—
Oex	-0.53912	—	—
Oe=	-0.53910	—	—
$-\mu\text{CH}_3\text{x}$	-0.12384	16	11
$-\mu\text{CH}_3=\text{}$	-0.12381	18	18
$+\mu\text{CH}_3\text{x}$	-0.12381	17	11'
$+\mu\text{CH}_3=\text{}$	-0.12379	15	12
$\text{x}\mu\text{CH}_3\text{m}$	-0.12379	14	10
$=\mu\text{CH}_3\text{m}$	-0.12373	13	9
+Me=	-0.12110	11	6
+Mex	-0.12108	8,9,10	3,4,5
$+\text{CH}_3\text{m}-$	-0.12102	1,3	1,2
$+\text{CH}_3=\text{}$	-0.11303	12	14
$-\text{CH}_3\text{x}$	-0.11285	6	13
$+\text{CH}_3\text{x}$	-0.11226	7	15
$=\text{CH}_3\text{m}+$	-0.11205	2	7
$\text{xCH}_3\text{m}+$	-0.11182	4	7'
$-\text{CH}_3=\text{}$	-0.11134	5	16
-Me=	-0.10900	8,9,10	3,4,5
-Mex	-0.10900	8,9,10	3,4,5
$-\text{CH}_3\text{m}-$	-0.10900	1,3	1,2
CH_2	-0.10019	19,21	17
CHe	-0.08289	22	27
$\mu_3\text{C}$	-0.02685	—	28
$\mu\text{CH}=\text{}$	-0.01435	24	19
μCHx	-0.01422	25	18
μCHm	-0.01411	23	20
CHx	+0.00610	28	23
$\text{CH}=\text{}$	+0.00610	27	22
$\text{CHm}-$	+0.00618	29	24
$\text{CHm}+$	+0.01318	26	21
Ce=	+0.04036	—	25
Cex	+0.04061	—	26
Tim	+2.30556	—	—
Ti=	+2.31537	—	—
Tix	+2.31555	—	—

length gives $T_1(\text{CHe}) = 161$ ms at 100.6 MHz and room temperature in CDCl_3 [$\tau_c = 277$ ps and $J(\omega) = 5.5$ ns]. This is not in good agreement with the experimental value [$T_1(\text{CHe}) = 850$ ms]. On the other hand using the $\langle R \rangle$ estimator [$\tau_c = 86$ ps and $J(\omega) = 1.7$ ns] under the same conditions leads to $T_1(\text{CHe}) = 512$ ms in much better agreement with the experimental value. In fact, in order to match the experimental value, a good choice would be $\langle R \rangle = 4.5$ Å [$\tau_c = 50$ ps and $J(\omega) = 996$ ps] leading to $T_1(\text{CHe}) = 884$ ms. Such a small reduction in size relative to a

Table 6 Predicted nuclear quadrupole coupling constants χ , asymmetry parameter η_Q and solution linewidth $\Delta\nu_{1/2}$ (54.24 MHz, CDCl_3 , $T = 298$ K) for the structural model of (2) shown in Fig. 12 (left)

Oxygen atom	χ/MHz	η_Q	$\Delta\nu_{1/2}/\text{Hz}^a$	$\Delta\nu_{1/2}/\text{Hz}^b$
$\mu_3\text{O}$	0.19	-0.01	3	1
$\mu\text{O}=\text{}$, μOx , μOm	9.4	1.8	15 300	4 800
Ox, O=, Om-	15.0	0	18 700	5 800
Om+, Oex, Oe=	15.1	0	19 000	5 900
Oe	17.2	0	24 700	7 700

^a Values computed using the largest dimension of the structural model ($R_{\text{max}} = 8.0$ Å, oblate-shaped molecule) corresponding to a rotational correlation time τ_c of 276.4 ps and a spectral density $J(\omega) = 276.3$ ps. ^b Values computed from the equivalent sphere of the structural model ($\langle R \rangle = 5.4$ Å) corresponding to a rotational correlation time τ_c of 86.1 ps and a spectral density $J(\omega) = 86.1$ ps.

$\langle R \rangle$ value computed from a rigid structure in a crystal is not unlikely considering thermal vibrations and interactions with solvent molecules in the condensed state. A good consistency check is then to use this $\langle R_{\text{eff}} \rangle$ value to estimate the T_1 relaxation time of the quite rigid methylene group located on the other side of the enolate ligand, leading to $T_1(\text{CH}_2) = 467$ ms, which compares extremely well with the experimental (437 ms) value. This allows us to complete Table 3 with the following estimated values: $T_1(\mu_3\text{C}) = T_1(\text{Cex}) = 22$ s, $T_1(\text{Ce=}) = 56$ s.

But the most interesting point is to apply this $\langle R_{\text{eff}} \rangle$ value to the methine groups of isopropoxy groups. Limiting ourselves to relaxation *via* the C-H bond would lead to a T_1 -value of 987 ms, while allowing additional relaxation *via* the six C-H bonds of the two *gem*-di-methyl groups would lead to a T_1 -value of 912 ms. A first conclusion is then that the observed difference $\Delta T_1 = +160$ ms between terminal and bridging isopropoxy groups may be explained by the fact that being more rigid, bridging groups may relax *via* all the H-atoms available within a sphere of radius 2.5 Å, whereas terminal ones relax only *via* the methine proton. An easy explanation for this higher rigidity of bridging isopropoxy groups is given in Fig. 13 (top) showing how the two components of the total energy are changing when a rotation of 360° is performed along the C-O bond axis. Referring to the dotted curve that corresponds to steric repulsive energy there is no secondary minimum in the bridging case (top left) in deep contrast with the terminal case (top right). After summation of both components we get an estimation of the activation energy for this whole rotation movement that is found to be $+612$ kJ mol⁻¹ for the bridging case and much smaller ($+95$ kJ mol⁻¹) for the terminal one. This means that a bridging isopropoxy is about 6 times more rigid than a terminal one. Similar activation energies may be evaluated for the other positions leading to $+637$ kJ mol⁻¹ ($\mu\text{CH}=\text{}$ site), $+646$ kJ mol⁻¹ (μCHx site), $+246$ kJ mol⁻¹ ($\text{CH}=\text{}$ site), $+109$ kJ mol⁻¹ (CHx site) and $+896$ kJ mol⁻¹ ($\text{CHm}+$ site). The pretty high rigidity for this last terminal group facing the enolate ligand is in part compensated by the possibility of undergoing chemical exchange with the $\text{CHm}-$ site that displays the lowest energy barrier.

A second conclusion drawn from these considerations on T_1 -values is that, owing to the rather large difference between experimental and theoretical values, isopropoxy groups are moving in a different time scale relative to the enolate ligand. This new time scale may be determined by looking at the τ_c value that should be used to recover the correct T_1 -value for terminal groups leading to $\tau_c = 27$ ps and $J(\omega) = 532$ ps. From this new τ_c -value, the missing T_1 -value of C22 may be evaluated as 1.85 s and a theoretical difference $\Delta T_1 = +140$ ms is expected between terminal and bridging positions in good agreement with experimental data. Referring to Fig. 13 these shorter correlation times may be related to the existence of a rather flat energy profile allowing libration movements with an amplitude of about $\pm 50^\circ$ around the minimum value. This possible libration movement is probably responsible for the difference in correlation times between the enolate ligand and the isopropoxy groups. Fig. 13 also shows the strong differentiation that exists between the two *gem*-di-methyl groups of isopropoxy ligands. As expected, activation energies for a whole rotation of 360° around the $\text{CH}-\text{CH}_3$ bond are considerably smaller. For bridging groups we got $+32$ kJ mol⁻¹ ($\text{x}\mu\text{CH}_3\text{m}$ site), $+25$ kJ mol⁻¹ ($+\mu\text{CH}_3\text{x}$ site), $+24$ kJ mol⁻¹ ($+\mu\text{CH}_3=\text{}$ site), $+16$ kJ mol⁻¹ ($-\mu\text{CH}_3\text{x}$ site), $+14$ kJ mol⁻¹ ($=\mu\text{CH}_3\text{m}$ site) and $+13$ kJ mol⁻¹ ($-\mu\text{CH}_3=\text{}$ site). In deep contrast with rotations along the C-O bonds, very similar activation energies are found for the terminal groups: $+26$ kJ mol⁻¹ ($+\text{Mex}$ site), $+25$ kJ mol⁻¹ ($+\text{Me}=\text{}$ site), $+17$ kJ mol⁻¹ ($+\text{CH}_3\text{m}-$ site), $+16$ kJ mol⁻¹ ($-\text{Mex}$ site), $+14$ kJ mol⁻¹ ($-\text{Me}=\text{}$ site), $+13$ kJ mol⁻¹ ($\text{xCH}_3\text{m}+$ site), $+8$ kJ mol⁻¹ ($=\text{CH}_3\text{m}+$ site) and $+4$ kJ mol⁻¹ ($-\text{CH}_3\text{m}-$ site). One may

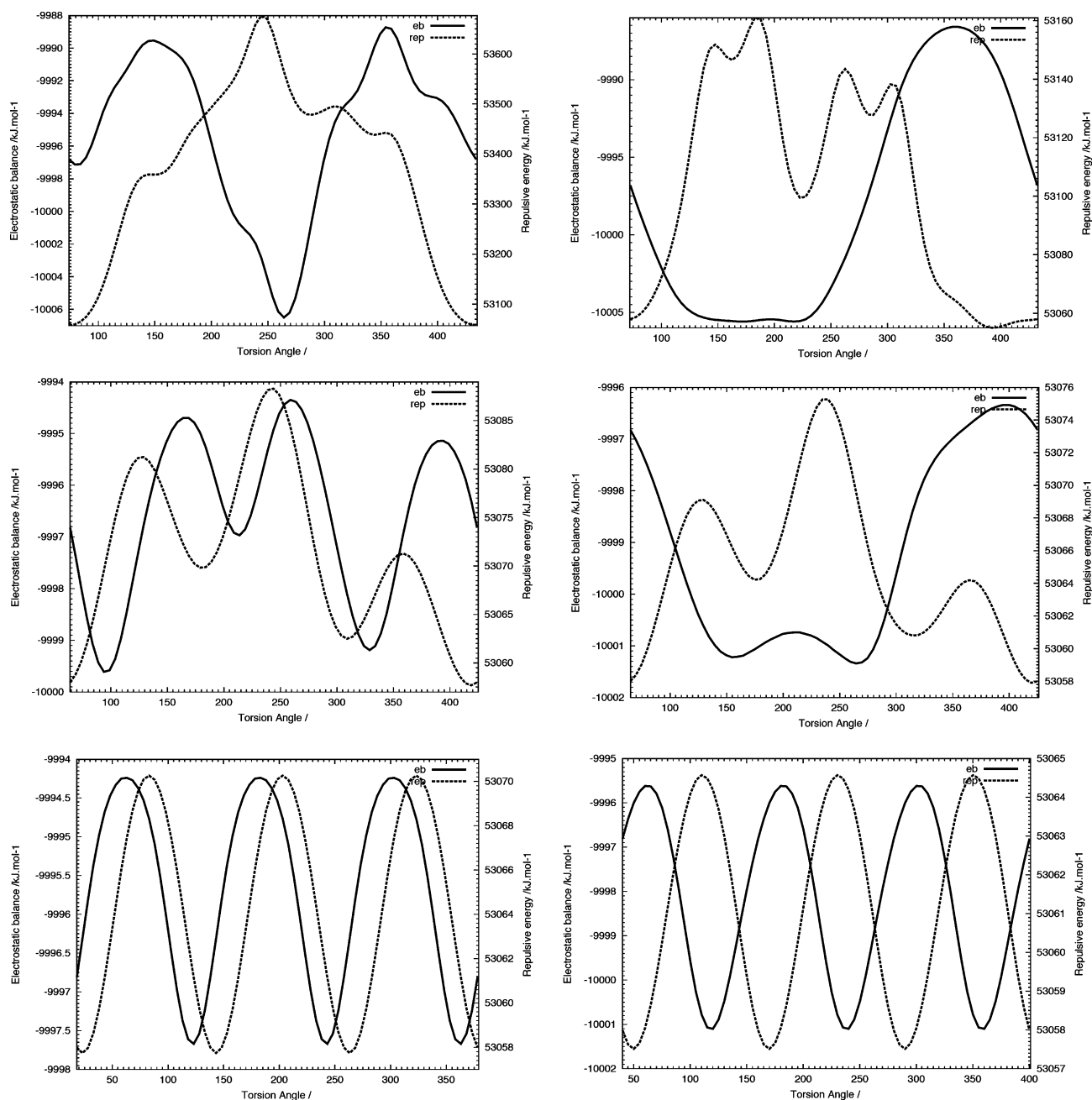


Fig. 13 Evolution of the two components of the total energy, repulsive plus dispersive (dotted line) and electrostatic (continuous line), when a rotation of 360° is performed along the C–O bond axis (top) or along the C–C bond (middle and bottom). Left part refers to a bridging and right part to a terminal isopropoxy group, both lying on the pseudo C_3 -symmetry axis. Quite similar curves are obtained for other positions and are not displayed here. The middle part refers to the methyl group that lies closest from the μ_3 -oxo group and the bottom part to the other *gem*-methyl group borne by the same methine group.

then expect a third kind of correlation time for these *gem*-dimethyl groups that should be about 15 ps [$J(\omega) = 295$ ps] and that corresponds to a full rotation along CH–CH₃ bonds. At last, the relaxation times of the *gem*-di-methyl groups are rather well explained by a τ_c -value close to 30 ps corresponding also to full rotations along C–CH₃ bonds. This is in line with computed activation energies of about +11 kJ mol⁻¹ with curves very similar in shapes to those displayed at the bottom right of Fig. 13.

Concerning ¹H relaxation times, the values for the methylene protons (experimental values at 450 ms) are rather well accounted for by the same overall correlation time used to interpret ¹³C relaxation times [$\tau_c = 50$ ps and $J(\omega) = 1.5$ ns, leading to $T_1(\text{CH}_2) = 555$ ms] provided that we include the geminal proton, the six H-atoms of the *gem*-di-methyl groups ($\pm\text{CH}_3\text{x}$) and the methine proton $\text{CHm}+$. For the methine groups of isopropoxy groups, we predict using $\tau_c = 27$ ps [*i.e.* $J(\omega) = 797$ ps] and looking at all H-atoms located within a

sphere of radius 5 Å: $T_1(\text{CHm}+) = 1.96$ s, $T_1(\text{CHx}) = T_1(\text{CH=}) = T_1(\text{CHm-}) = 1.64$ s, $T_1(\mu\text{CHm}) = T_1(\mu\text{CH=}) = 1.41$ s and $T_1(\mu\text{CHx}) = 1.20$ s in rather good agreement with experimental values (Table 3). The experimental difference of about +200 ms between terminal and bridging isopropoxy groups is thus clearly related to the molecular structure, a very satisfying result. At last for methyl groups using $\tau_c = 15$ ps [*i.e.* $J(\omega) = 443$ ps] we predict T_1 -values of about 700 ms, again in good agreement with Table 3. This demonstrates the overall coherence of the proposed structural model for (2) that fully accounts for both static and dynamic properties of this complex.

Conclusion and perspectives

To sum up, this study was undertaken owing to the systematic isolation as single-crystals of complexes (2) or (4) when

titanium(IV) isopropoxide (**1**) was reacted with widely different ligands such as 1,3-propanediol, 2,2'-biphenol or triphenylacetic acid using acetone as a solvent. As all these ligands are known to display a strong affinity for Ti(IV) centres, these were rather surprising results. Recording of ^{17}O NMR spectra after dissolution of these crystals in chloroform has evidenced at least three kinds of μ_3 -oxo groups. It was then proposed that the systematic disorder observed in the crystalline state was due to a complex intergrowth between (**2**), (**3**) and (**4**) that share the same $[\text{Ti}_3(\mu_3\text{-O})(\mu\text{-OPr}^i)_3]$ core and not to a single complex (**2**) offering three kinds of possible coordination sites for a tridentate enolate ligand. As this complex behaviour was not considered in previous studies, a full characterisation of (**2**) using ^1H , ^{13}C and ^{17}O NMR spectroscopies was undertaken. As (**2**) displays one of the most simple structures for an oxo-alkoxide system, it was thus possible to firmly establish using a non-empirical modelling of the molecular structure of (**2**) that more shielded ^1H and ^{13}C resonances and shorter relaxation times were expected for more rigid bridging OR groups relative to terminal ones. Also, the importance of the simultaneous use of HSQC, HBMBC and ROESY techniques for a full spatial attribution of all resonances and the existence of several correlation times ($\tau_c = 50$ ps for overall rotation, $\tau_c = 27$ ps for libration along C–O bonds and $\tau_c = 15$ ps for full rotation along CH–CH₃ bonds) within the same complex have been demonstrated. Concerning the ^{17}O nucleus, quadrupolar coupling constants larger than 10 MHz were predicted for C-bonded oxygen atom increasing in the order $\mu\text{-OR} < \eta^1\text{-OR}$ (i.e. terminal OR) $< \mu_3\text{-OR}$. Much smaller constants were predicted for oxo groups. Consequently, even if it is not yet possible to compute directly ^{13}C NMR chemical shifts from the molecular structure, it remains nevertheless that a full assignment, based on 2D experiments and not on theory, of NMR resonances of (**2**) has been proposed. It may then be anticipated that (**2**) should become a benchmark compound for further theoretical studies devoted to the prediction of ^{13}C NMR chemical shifts in oxo-alkoxide systems.

Returning to chemistry, we feel (but that remains to be clearly demonstrated) that the systematic appearance of (**2**) in the presence of a wide range of ligands is a kinetic effect linked to the steric decompression that may occur when the rather constrained molecular structure of (**3**) meets acetone molecules under their enol form: $(\mathbf{3}) + 3 \text{CH}_2=\text{C}(\text{OH})\text{CH}_3 \rightarrow (\mathbf{2}) + 3 \text{HOPr}^i$. The fact that such a reaction occurs only with acetone molecules allows us to speak of molecular templating and readily explains why exactly three acetone molecules should undergo aldol condensation. Viewing (**2**) or (**5**) as kinetic products is suggested by the extreme difficulty of obtaining large yields of (**5**) and by the isolation in this system of other single-crystals upon aging of the mother solutions. These new molecular structures are under investigation and will be reported elsewhere. The low yields obtained for (**5**) associated with rather complex NMR spectra and the large yields characterising the much simpler compound (**2**) also explain why the full NMR study focussed on an already known product (**2**) and not on the new one (**5**). Much work remains to be done to find good experimental conditions favouring (**5**) over (**2**).

Acknowledgements

Many thanks are due to the Strasbourg NMR team (Francis Taulelle, Roland Graf, Lionel Allouche, Jean-Daniel Sauer, Maurice Coppe) for their assistance in recording and interpreting NMR data. We are also indebted to André DeCian, Nathalie Kyritsakas and Jean-Marc Planeix, for their assistance in recording single-crystal X-ray data and crystal structure determination. This work was realised at Université

Louis Pasteur with public funds allocated by CNRS and the French government.

References

- M. Henry, in *Handbook of Organic–Inorganic Hybrid Materials and Nanocomposites*, ed. H. S. Nalwa, American Scientific Publishers, Stevenson Ranch, 2003, pp. 1–82.
- J. Livage, M. Henry and C. Sanchez, *Prog. Solid State Chem.*, 1988, **18**, 259.
- K. Gigant, A. Rammal and M. Henry, *J. Am. Chem. Soc.*, 2001, **123**, 11632.
- A. Rammal, F. Brisach and M. Henry, *J. Am. Chem. Soc.*, 2001, **123**, 5612.
- S. Weymann-Schildknecht and M. Henry, *J. Chem. Soc., Dalton Trans.*, 2001, 2425.
- F. Biechel, J. Dubuc and M. Henry, *New J. Chem.*, 2004, in press.
- A. Rammal, F. Brisach and M. Henry, *C. R. Chim.*, 2002, **5**, 59.
- J. A. Ibers, *Nature*, 1963, **197**, 686.
- D. A. Wright and D. A. Williams, *Acta Crystallogr., Sect. B*, 1968, **24**, 1107.
- M. Henry, *ChemPhysChem*, 2002, **3**, 561.
- V. W. Day, T. A. Eberspacher, W. G. Klemperer, C. W. Park and F. S. Rosenberg, *J. Am. Chem. Soc.*, 1991, **113**, 8190.
- V. W. Day, T. A. Eberspacher, Y. Chen, J. Hao and W. G. Klemperer, *Inorg. Chim. Acta*, 1995, **229**, 391.
- J. Blanchard, F. Ribot, C. Sanchez, P.-V. Bellot and A. Trokner, *J. Non-Cryst. Solids*, 2000, **265**, 83.
- T. J. Boyle, T. M. Alam, E. R. Mechenbier, B. L. Scott and J. W. Ziller, *Inorg. Chem.*, 1997, **36**, 3293 and references therein.
- J. V. Barkley, J. C. Cannadine, I. Hannaford, M. M. Harding, A. Steiner, J. Tallon and R. Whyman, *Chem. Commun.*, 1997, 1653.
- N. Steunou, F. Ribot, K. Boubekeur, J. Maquet and C. Sanchez, *New J. Chem.*, 1999, **23**, 1079.
- A. A. Shaw, C. Salaun, J.-F. Dauphin and B. Ancian, *J. Magn. Reson. A*, 1996, **120**, 110.
- B. Ancian, I. Bourgeois, J.-F. Dauphin and A. A. Shaw, *J. Magn. Reson. A*, 1997, **125**, 348.
- H. Desvaux, P. Berthault, N. Birlirakis, M. Goldman and M. Piotto, *J. Magn. Reson. A*, 1995, **113**, 47.
- L. E. Kay, P. Keifer and T. Saarinen, *J. Am. Chem. Soc.*, 1992, **114**, 10663.
- A. Bax and M. F. Summers, *J. Am. Chem. Soc.*, 1986, **108**, 2093.
- M. Henry, *ChemPhysChem*, 2002, **3**, 607.
- M. Henry, *J. Cluster Sci.*, 2002, **13**, 437.
- M. Henry, *J. Cluster Sci.*, 2003, **14**, 267.
- L. Beitone, J. Marrot, T. Loiseau, G. Férey, M. Henry, C. Huguenard, A. Gansmuller and F. Taulelle, *J. Am. Chem. Soc.*, 2003, **125**, 1912.
- L. Beitone, C. Huguenard, A. Gansmuller, M. Henry, F. Taulelle, T. Loiseau and G. Férey, *J. Am. Chem. Soc.*, 2003, **125**, 9102.
- A. Müller and M. Henry, *C. R. Chim.*, 2003, **6**, 1201.
- M. Henry, F. Taulelle, T. Loiseau, L. Beitone and G. Férey, *Chem. Eur. J.*, 2004, **10**, 1366.
- T. Loiseau, C. Serre, C. Huguenard, G. Finkh, F. Taulelle, M. Henry, T. Bataille and G. Férey, *Chem. Eur. J.*, 2004, **10**, 1373.
- J. M. Douillard and M. Henry, *J. Colloid Interface Sci.*, 2003, **263**, 554.
- M. Henry, *Solid State Sci.*, 2003, **5**, 1201.
- M. Henry, *Am. Chem. Soc. Symp. Ser.*, 1999, **732**, 277.
- T. M. Alam and M. Henry, *Phys. Chem. Chem. Phys.*, 2000, **2**, 23.
- M. Henry, *WinPacha V2.5 software*, 1993–2004, <http://www-chimie.u-strasbg.fr/~lcmes/chimist> (click on link Pacha). A tutorial (French only!) is also available (Windows only!) as well as a very limited help file in English. Further help may be obtained by sending an e-mail to henry@chimie.u-strasbg.fr.
- J. E. Nordlander, A. F. Bond, IV and M. Bader, *Comput. Chem.*, 1985, **9**, 209.
- W. H. Press, S. A. Teukolsky, W. T. Vetterling and B. P. Flannery, *Numerical recipes in C*, 2nd edn., Cambridge University Press, New York, 1992, p. 444.
- M. A. Spackman, *J. Chem. Phys.*, 1986, **85**, 6579.
- F. Cleri and V. Rosato, *Phys. Rev.*, 1993, **48**, 22.
- E. A. C. Lucken, *Nuclear quadrupole coupling constants*, Academic Press, New York, 1969.
- R. G. Barnes and W. V. Smith, *Phys. Rev.*, 1954, **93**, 95.
- C. P. Cheng and T. L. Brown, *J. Am. Chem. Soc.*, 1979, **101**, 2327.
- A. Carrington and A. D. McLachlan, *Introduction to Magnetic Resonance*, Harper & Row, New York, 1969.

-
- 43 A. Bondi, *J. Phys. Chem.*, 1964, **68**, 441.
44 C. J. Jameson and H. S. Gutowsky, *J. Chem. Phys.*, 1964, **40**, 1714.
45 W. H. Flygare and J. Goodisman, *J. Chem. Phys.*, 1968, **49**, 3122.
46 K. M. S. Saxena and P. T. Narasimhan, *Int. J. Quantum Chem.*, 1967, **1**, 731.
47 A. K. Jameson and C. J. Jameson, *Chem. Phys. Lett.*, 1987, **134**, 461.
48 J. Vaara, J. Lounila, K. Ruud and T. Helgaker, *J. Chem. Phys.*, 1998, **109**, 8388.
49 H. A. Christ, P. Diehl, H. R. Schneider and H. Dahn, *Helv. Chim. Acta*, 1961, **44**, 865.
50 S. Doeuff, Y. Dromzee, F. Taulelle and C. Sanchez, *Inorg. Chem.*, 1989, **28**, 4439.
51 A. Gavezzotti, *J. Am. Chem. Soc.*, 1983, **105**, 5220.